FEDERAL UNIVERSITY OF SANTA CATARINA
JOINVILLE TECHNOLOGY CENTER
UNDERGRADUATE COURSE IN MECHATRONICS ENGINEERING

GUILHERME ARAUJO MACHADO DO NASCIMENTO

MODELING THE HEATING PROCESS IN THE MACHINE FOR PRECISION GLASS MOLDING

Joinville
2023

GUILHERME ARAUJO MACHADO DO NASCIMENTO

MODELING THE HEATING PROCESS IN THE MACHINE FOR PRECISION GLASS MOLDING

This graduation thesis is presented to fulfill the partial requirement to obtain the title of bachelor in the course of Mechatronic Engineering, at the Joinville Technology Center, from the Federal University of Santa Catarina.
Supervisor: Prof. Benjamin Grando Moreira, Dr.
Co-supervisor: Cheng Jiang, M. Sc.

Joinville
2023

Ficha de identificação da obra elaborada pelo autor,
através do Programa de Geração Automática da Biblioteca Universitária da UFSC.

Nascimento, Guilherme Araujo Machado do
Modeling the heating process in the machine for Precision Glass Molding / Guilherme Araujo Machado do Nascimento ; orientador, Benjamin Grando Moreira, coorientador, Cheng Jiang, 2023.
57 p.

Trabalho de Conclusão de Curso (graduação) - Universidade Federal de Santa Catarina, Campus Joinville, Graduação em Engenharia Mecatrônica, Joinville, 2023.

Inclui referências.

1. Engenharia Mecatrônica. 2. PID controller. 3. System Identification. 4. Precision Glass Molding. I. Moreira, Benjamin Grando. II. Jiang, Cheng. III. Universidade Federal de Santa Catarina. Graduação em Engenharia Mecatrônica. IV. Título.

Guilherme Araujo Machado do Nascimento

Modeling the Heating Process in the Machine for Precision Glass Molding

This dissertation was evaluated in the context of the subject EMB5045 (Bachelor Thesis) and approved in its final form by the Undergraduate Course in Mechatronics Engineering

Joinville, 28th of June, 2023.

Prof. Benjamin Grando Moreira, Dr.
Course Coordinator

Examining Board:

Prof. Benjamin Grando Moreira, Dr.
University Advisor
Federal University of Santa Catarina

Cheng Jiang, M. Sc.
Company Supervisor
Fraunhofer-Institut für Produktionstechnologie

Prof. Pablo Andretta Jaskowiak, Dr.
Evaluator
Federal University of Santa Catarina

Prof. Alexandro Garro Brito, Dr.
Evaluator
Federal University of Santa Catarina

ACKNOWLEDGEMENTS

First of all I would like to thank my parents for the unconditional love and support they have always given me, helping me to follow my dreams. A big thank you to my sister, for being there for me at all times, always ready to help me, whether it was with schoolwork when I was younger or with life advice as I got older, whether it was to understand how does a mitochondria work or if I should move to another country, you are a role model for me. Being the older sibling is hard, but you do a great job at it.

I would also like to thank all my friends from UFSC Joinville, who have been through this journey with me from the beginning, for all the moments we have shared with each other, the hours spent studying at the university, the liters of coffee drank in the cafeteria, the Christmas parties at the end of the year, thank you for making the graduation a little less stressful. To all the friends I made during my stay in Aachen, the time spent here was an incredible experience and I will take everyone of you in my mind wherever I go. You were my family in times when the distance to my home country was too long to count.

Lastly, but not least, I would like to thank Cheng, for accepting me as a student assistant at Fraunhofer, giving me the opportunity to grow both personally and professionally, and for all the intensive help during this challenging work. Thanks also to Benjamin, for accepting to be my supervisor and a special thanks to Pablo, for giving me the first opportunity many years ago, which helped me, directly and indirectly, gain the experience that brought me here today.

ABSTRACT

Precision Glass Molding is an important technique to be used in the production of optical components, such as glass lenses. Along with that, since it is a complex procedure and it involves complex domains, a common method used to simulate the machine parts, boundary conditions and applied forces is the Finite Element Method. A Toshiba machine coupled with a Proportional-Integral-Derivative controller is responsible for the execution of the molding process, in which a series of steps are performed, such as heating, soaking, compression and cooling. The proposed work has the focus on the heating portion and the goal of modeling the system, in order to optimize the process parameters and obtain simulation results with even more precision. Inside the machine, infrared lamps are responsible for heating the tools, by emitting radiation. An assumption is that by accurately modelling the system, the temperature can be controlled without the need of the lamps in the FEM simulation. The presented thesis consists in multiple steps, such as applying control techniques, as well as system identification methods, to find an adequate representation of the real system, simulate the model and validate with experimental data, and perform experiments in the FEM software using the results from the model. The predicted model performed well against experimental data considering the desired margins of error, using the same PID parameters from the machine, which proved that the model can describe the system.

Keywords: PID Controller. FEM Simulation. System Identification. Precision Glass Molding.

RESUMO

A Moldagem de Vidro de Precisão é uma técnica muito importante a ser usada na produção de componentes ópticos, como lentes de vidro. Junto com isso, um método comum usado para simular o procedimento, as peças da máquina, as condições de contorno e as forças aplicadas é o Método dos Elementos Finitos. Uma máquina Toshiba acoplada a um controlador Proporcional-Integral-Derivativo é responsável pela execução do processo de moldagem, no qual uma série de etapas é realizada, como aquecimento, imersão, compressão e resfriamento. O trabalho proposto tem como foco a etapa de aquecimento e o objetivo de modelar o sistema, a fim de otimizar os parâmetros do processo e obter resultados de simulação com ainda mais precisão. No interior da máquina, lâmpadas infravermelhas são responsáveis pelo aquecimento das ferramentas, emitindo radiação. Uma suposição é que, ao modelar o sistema com precisão, a temperatura pode ser controlada sem a necessidade das lâmpadas. O trabalho apresentado consiste em várias etapas, como a aplicação de técnicas de controle, bem como métodos de identificação de sistema, para encontrar uma representação adequada do sistema real, simular o modelo e validá-lo com dados experimentais e realizar experimentos no software de FEM usando os resultados do modelo. O modelo obtido teve um bom desempenho em comparação com os dados experimentais, usando os mesmos parâmetros do PID da máquina, o que provou que o modelo pode descrever o sistema com precisão.

Palavras-chave: Controlador PID. Simulação FEM. Identificação de Sistema. Modelagem de Precisão de Vidro.

LIST OF FIGURES

LIST OF TABLES

LIST OF ABBREVIATIONS AND ACRONYMS

API	Application Programming Interface
ARX	AutoRegressive with eXternal input
CAD	Computer-Aided Design
ERA	Eigensystem Realization Algorithm
FEM	Finite Element Method
HTTP	HyperText Transfer Protocol
IPT	Institute for Production Technology
LTI	Linear Time-Invariant
MIMO	Multiple Input Multiple Output
NARX	Nonlinear ARX
NRMSE	Normalized Root Mean Squared Error
OKID	Observer Kalman Filter Identification
PGM	Precision Glass Molding
PID	Proportional-Integral-Derivative
SISO	Single Input Single Output
SVD	Singular Value Decomposition
UML	Unified Modeling Language

LIST OF SYMBOLS

$e(t)$	Error signal
$u(t)$	Input signal
$y(t)$	Output signal
$r(t)$	Reference signal

CONTENTS

1 INTRODUCTION

The production of optical glass lenses consists of using machining processes, such as grinding, polishing and lapping, which can have a high cost and time consumption, especially when the lenses have complex features. Therefore, Precision Glass Molding (PGM) has been developed to achieve a more efficient way of manufacturing these complex optical components (ZHANG, L.; LIU, W., 2017).

Digital cameras, phone cameras as well as CD and DVD players are some of the applications for aspherical optical elements. Since they can be produced quickly and cheaply on a wide scale, polymer-based lenses are used in the majority of these applications, but because glass has better optical features than polymers, precision glass optics are in higher demand (IQBAL, 2009).

Even though glass molding has many advantages in comparison with a traditional machining process, some difficulties may be encountered in case some details are not taken into consideration. The process needs to be performed above the glass transition temperature, where the material has an unstable non-equilibrium structure. Besides that, PGM method is susceptible to the molding temperature, since the glass viscosity can vary within a constrained range of permissible temperature variation (ZHANG, L.; LIU, W., 2017).

Glass molding is a practical method for creating complex-shaped, precise micro structured optical devices with excellent production efficiency. Modelling the heat transfer and high-temperature deformation behavior of glass is a crucial subject because glass deforms at high temperatures, where the mechanical and optical properties are substantially temperature dependent (YAN et al., 2009).

Overall the process, shown in Figure 1, consists first in loading a preform glass with a selected shape in the machine, followed by heating, soaking, molding, cooling, demolding and once again cooling (ZHANG, L.; LIU, W., 2017). During the heating stage, infrared lamps are responsible for emitting radiation into the system, raising the temperature in the machine to a determined value.

Figure 1 – A simplified PGM process.

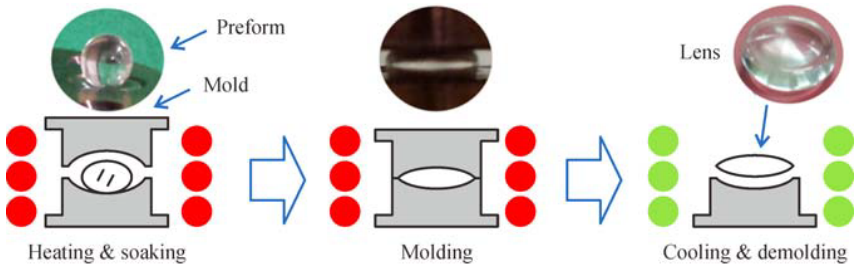

Source: Zhang (2017, p. 6)

To control the temperature to a desired value with a established margin of error, a Proportional-Integral-Derivative (PID) controller is used based on the input process parameters. In the machine, the tools temperature can be controlled based on the lamp power, but in the Finite Element Method (FEM) simulation it is not possible to use power as an input to the existing model, which results in an inaccurate performance.

Currently it is not possible to know the exact temperature of the infrared lamps in the heating step of the PGM process, only the power values are measurable, but it is not possible to use power as a boundary condition in the FEM simulation. In addition to that, a change in the temperature values in the machine can cause a change in the PID parameters, and tuning the controller consumes a lot of time, since it takes around half an hour for the machine to run an experiment. Therefore, a correlation between lamp power and tool temperature as well as modelling a system to simulate and control the tool temperature is necessary in order to solve these problems.

1.1 OBJECTIVES

In order to solve the mentioned problems, the following objectives are proposed.

1.1.1 General Objective

The general objective of the present work is to identify a correlation between lamp power and tools' temperatures in the heating step and to analytically model a PID to control the temperature of the infrared lamps, based on the input process parameters and output power data from the experiments.

1.1.2 Specific Objectives

- Build the already existing digital twin for the PGM process;
- Identify the correlation between lamp power and tool temperature;
- Model a PID to control the tool temperature, based on the input process parameters and experimental power data;
- Validate the model by comparing with experimental results.

1.2 THE RESEARCH INSTITUTE

This work was produced in the Fraunhofer Institute for Production Technology (IPT), located in the *Rheinisch-Westfälische Technische Hochschule* Campus, in the city of Aachen, North Rhine-Westphalia, Germany. The institute, founded in 1980 by Wildfried König, is an institution from *Fraunhofer-Gesellschaft* and promotes applied research.

The institute has a focus on process technology, production quality and metrology, production machines and technology management, developing systems solutions for manufacturing companies. The basis of the institute also consists in developing and optimizing methods, technologies and processes for production (IPT, 2022b).

The department of Fine Machining and Optics is responsible for the production and machining of precision components, researching and developing technologies, such as automated fine machining, diamond cutting and ultra-precision grinding. Some other technologies includes polishing, micro- and nanastructuring and molding of high-precision glass optics (IPT, 2022a).

1.3 OUTLINE

The present report describes the state of the art (Chapter 2), the methodology (Chapter 3), the results (Chapter 4), the conclusion (Chapter 5), and the summary.

2 STATE OF THE ART

This section describes the background knowledge necessary for the present work.

2.1 PRECISION GLASS MOLDING

PGM is a replicative technology that enables the creation of highly precise optical components from glass without the need for grinding or polishing. Also known as ultra-precision glass pressing, the process has a wide range of applications, including those for automotive and digital cameras. The first one accounted in 2018 for approximately 60% of the market, and it will continue to be the primary application in the upcoming years (24CHEMICALRESEARCH, 2019).

The process is a practical fabrication technique for complex-surfaced optics at high temperatures under isothermal circumstances. However, in actual molding, it is difficult to establish a consistent temperature distribution for molds and glass preforms due to flaws in mold design and rigid temperature control of the molding process (ZHANG, Y.; LIANG; MILSTER, 2021).

By first heating the glass raw material to a temperature above its transition temperature and then pressing it between optically polished molds to make a lens, PGM is a hot forming method. After molding, a controlled cooling process is used with a preset holding force to eliminate any remaining strains and thermal shrinkage brought on by a drop in temperature (DAMBON et al., 2009).

In more details, the steps can be divided in five cycles, as shown in Figure 2, which are:

1. Heating step: The first step is to position the glass preform into the molds. In order to remove oxygen from the machine and avoid oxidation, vacuum or nitrogen purging is used. Sequentially, the temperature is elevated until it exceeds only by a small amount the glass transition temperature of the glass material (IQBAL, 2009);

2. Soaking step: To maintain uniform material characteristics and the same temperature across the entire glass surface, in this step the temperature in the machine is hold at a constant value. This process gives enough time for the glass to become more visco-elastic, which allows it to be shaped and molded as desired (IQBAL, 2009);

3. Compression step: Using the same temperature as the previous cycle, the compression step consists in applying a constant force to each half of the molds,

Figure 2 – PGM steps.

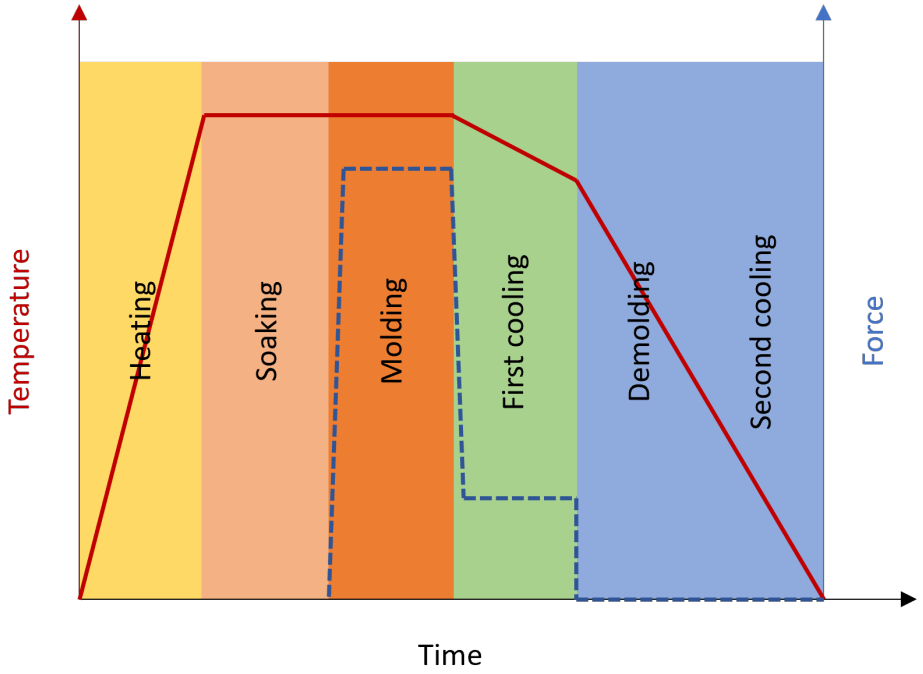

Source: Zhang (2017, p. 5)

compressing the glass gob in order to shape it accordingly to the upper and lower molds (IQBAL, 2009);

4. Slow cooling step: Also known as annealing, this step is responsible for avoiding internal stresses during the process. This cycle is important because it can prevent any distortion or cracking, due to a gradient in the temperature or a mechanical shock, resulting in a bad quality in imaging in the final lens. In order to increase the heat transfer by convection, nitrogen gas is used during this process (IQBAL, 2009);

5. Fast cooling step: After heating and slowly cooling the lens, cooling in a higher drop rate is executed to bring the mold and the lens to a safe temperature, which means, a temperature where they can be removed from the machine safely. To achieve this effective cooling, the chamber is filled with nitrogen at a high flow rate, while the heating components are deactivated (IQBAL, 2009).

2.2 FINITE ELEMENT METHOD

The transformation of partial differential equations into algebraic equations, using an approximation of variables that are uncertain or not known, is what defines FEM. Commonly used for describing physical laws with partial differential equations,

in numerical methods to elaborate and solve algebraic equations or to do calculations more efficiently, with the help of a computer. In industrial applications, the method is most of the times combined with other tools for the pre-processing of the data and also to analyze the results, such as a Computer-Aided Design (CAD) software (DHATT; LEFRANÇOIS; TOUZOT, 2012).

Since the 1950s and 1960s, the aerospace industries have extensively developed and used FEM, which has its roots in the field of structural analysis, also frequently employed by mechanical engineers, especially for the analysis of stress in solid components. In this method, physical systems like structures, solids or fluids must be divided into tiny sub-regions or components. Each component is a fundamentally straightforward unit whose behavior is easily understood. Instead of applying the difficult mathematics required by many analytical solutions, the complexity of the systems is adapted by using a vast number of elements (FENNER, 2013).

Differential equations, a key tool in the quantitative sciences, are used to describe a variety of events. However, the vast majority of these differential equations lacks an analytical solution, hence to address the issue a numerical solution is proposed. One of the most common techniques employed for this purpose is the FEM. There are three main properties that justify the popularity of it, being them the ability to handle arbitrary shaped domains, the capacity of effortlessly handling boundary conditions and the possibility of increasing the accuracy of the solution results, by either turning the elements smaller or increasing the degree of the polynomial that calculates the approximation in the element (WHITELEY, 2017).

Two important rules need to be satisfied when dividing a domain into smaller components. The first rule is that two components with existing common boundaries between them can have common points only on these boundaries, which can be points, lines or surfaces. Another rule that needs to be followed is that the domain cannot have any empty space between the components, which means that the collection of elements must create a domain that closely resembles the original domain (DHATT; LEFRANÇOIS; TOUZOT, 2012).

2.3 HEAT TRANSFER

As stated by Levenspiel (2014), in general, there are three different ways that heat can move from one place to another: conduction, convection and radiation.

2.3.1 Conduction

The heat transfer through direct molecular contact between the hotter and cooler parts of a body is referred to as conduction (LEVENSPIEL, 2014). Fourier's law, Equation (1), describes how the rate of heat transfer in steady state relies on the types of

materials used and the temperature differences between them

$$\dot{q_x} = -kA\frac{dT}{dx}\left[\frac{J}{s} = W\right]. \tag{1}$$

The temperature gradient in the x direction is represented by $\frac{dT}{dx}\left[\frac{K}{m}\right]$; $A[m^2]$ denotes the area perpendicular to the direction of heat flow; $k\left[\frac{W}{mK}\right]$ represents the thermal conductivity; and $\dot{q_x}[W]$ is the rate of heat transfer in the horizontal direction. The negative sign in this equation indicates that heat moves from the hotter regions to the cooler ones, in accordance with the second law of thermodynamics (LEVENSPIEL, 2014).

In steady-state heat conduction without heat generation, the equation can be described in any direction through an isotropic material, as shown in Equation (2)

$$\dot{q} = -kA(\Delta T). \tag{2}$$

2.3.2 Convection

The heat transfer occasioned by fluids in movement is known as convection. When a fluid is moving, it may come into contact with different types of fluids or solid surfaces, which have different temperatures. As a result, the behavior of heat convection between flowing fluids and solid surfaces is triggered (DONG; LIU, H.; CHEN, 2021).

Considering a fluid moving through or above a surface with thickness of boundary layer δ, illustrated by Figure 3, the heat transfer can be represented by Equation (3) (LEVENSPIEL, 2014).

$$\dot{q} = -kA\frac{\Delta T}{\delta} = -hA\Delta T, \tag{3}$$

where $h = k/\delta$ is the heat transfer coefficient, in W/m^2K.

2.3.3 Radiation

Electromagnetic waves are responsible for heat transfer by thermal radiation, phenomenon that happens in vacuum or in substances that permit the transmission of those waves. Radiation does not require a medium, in contrast to heat conduction,

Figure 3 – Convection heat transfer.

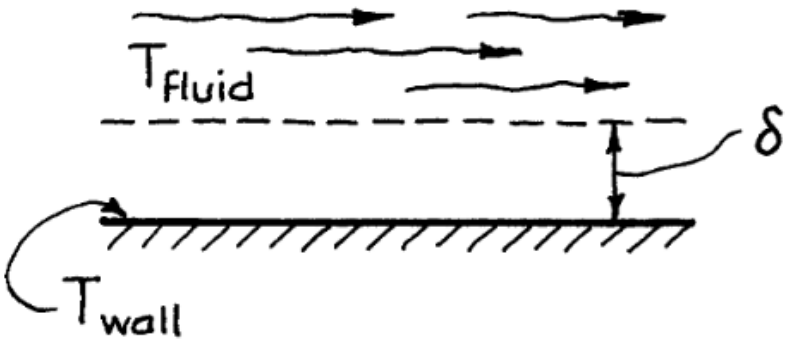

Source: Levenspiel (2014, p. 184)

which manages the transfer via the movement of molecules, atoms or electrons and hence requires a transfer medium (BÖCKH; WETZEL, 2012).

A "black body", which is described as a perfect emitter, since it absorbs all incident radiation, emits energy in form of radiation with a rate given by Equation (4)

$$Q = A\sigma T^4. \tag{4}$$

The Stefan-Boltzmann constant, named after the physics Josef Stefan and Ludwig Boltzmann, is represented by the greek letter σ and has a constant value of $5.66961 \times 10^{-8} \frac{W}{m^2 K^4}$. The variable T is the emitter absolute temperature, in Kelvin, and A is the surface area. For other bodies that are not perfect emitters, an emissivity factor is also included, as stated by Equation (5) (BURMEISTER, 1993)

$$Q = \epsilon A\sigma T^4, \tag{5}$$

where ϵ is the emissivity and $0 \leq \epsilon \leq 1$.

2.4 PID CONTROLLER

The most common industrial controllers are PID controllers. A control network with a PID control module as its primary control building block can be found even in the

most complex industrial control systems. It has been in use for a very long time and has successfully weathered the transition from the analogue to the digital computer control system eras of technology (JOHNSON, 2005).

This type of controller is composed of three components. The first term *P* stands for Proportional, the term *I* stands for Integral and *D* means the Derivative portion. The representation in time of the three portions of the controller is shown in Equation (6)

$$u(t) = K_p e(t) + \int_0^t K_i e(t)dt + K_d \frac{de(t)}{dt}, \tag{6}$$

where $e(t)$ is the calculated error value from the feedback loop and $u(t)$ is the control variable. Each portion of the Equation (6) will be explained from Sections 2.4.1 to 2.4.3. After applying Laplace transformation to obtain the transfer function of the controller, the representation of the PID can be illustrated in Figure 4

Figure 4 – PID Controller.

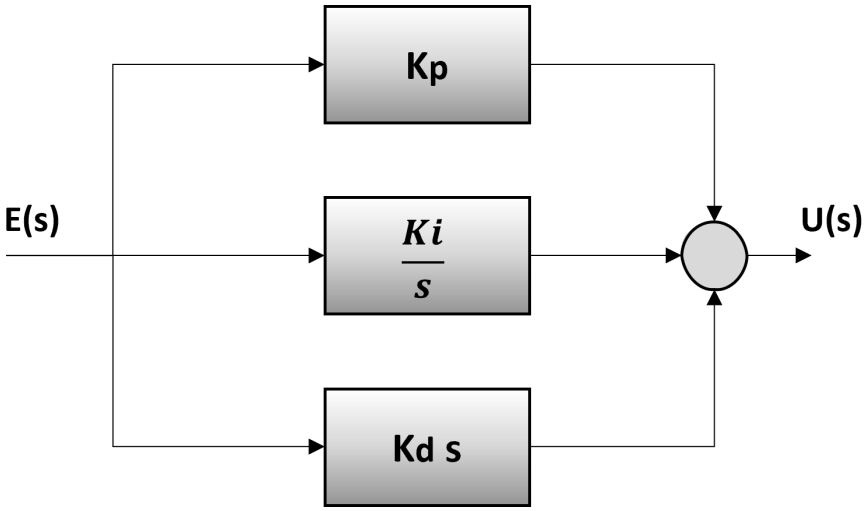

Source: Author

This controller acts on the system error $E(s)$ by the three different control actions, each with a specific objective, and the sum of these three terms outputs the signal $U(s)$, as shown in Figure 4 and represented by Equation (7)

$$\frac{U(s)}{E(s)} = K_p + \frac{K_i}{s} + K_d s. \tag{7}$$

By increasing or decreasing the K_p, K_i or K_d values, a different effect is obtained in the control system and its response, both transient and steady state. Table 1 represents the result of the changes in each term of the controller, illustrating how some system performance specifications changes when the PID parameters are increased

Table 1 – PID performance specifications.

Parameter	**Rise Time**	**Overshoot**	**Settling Time**	**Steady State Error**	**Stability**
K_p	$\downarrow$	$\uparrow$	Small change	$\downarrow$	$\downarrow$
K_i	$\downarrow$	$\uparrow$	$\uparrow$	0	$\downarrow$
K_d	Minor change	$\downarrow$	$\downarrow$	No effect	$\uparrow$, if K_d is small

Source: Musa (2018).

2.4.1 Proportional term

The proportional term relates to static gain. This portion operates on the error signal at the current time, sending a command action proportional to the error found. The greater the determined error, the more effective will be the control action due to this term. Besides that, this control action does not take into account past conditions of the error signal, only what occurs at the current moment. This portion is represented by Equation (8)

$$u(t) = K_p e(t). \tag{8}$$

By applying the Laplace transform in Equation (8), the proportional action can be represented as a proportional static gain K_p, as shown in Equation (9)

$$\frac{U(s)}{E(s)} = K_p. \tag{9}$$

2.4.2 Integral term

This term operates on the integral of the error signal, by acting on remaining errors from previous periods, not yet corrected. The greater the presence of remaining errors, the more intense its action, which is to correct persistent errors. This action is

seen as a correction on the past history of the system error, with a focus on the steady-state and a slow response to the current error. This portion is usually represented by Equation (10)

$$u(t) = \int_0^t K_i e(t) dt. \tag{10}$$

Once again, by applying Laplace transform, the integral term can be written as Equation (11)

$$\frac{U(s)}{E(s)} = \frac{K_i}{s}. \tag{11}$$

2.4.3 Derivative term

This action operates on the derivative of the error signal, acting on the trend of evolution of this signal. If the error presents an increasing trend, the control action is more intense. Otherwise, if the trend is downward, the action is less intense. This is seen as a correction to the future history of the control system's error, since it acts on its tendency to evolve. The focus here is on the transient response. This portion is usually represented by Equation (12)

$$u(t) = K_d \frac{de(t)}{dt}. \tag{12}$$

The derivative term can also be represented by the equivalent after Laplace transformation, as shown in Equation (13)

$$\frac{U(s)}{E(s)} = K_d s. \tag{13}$$

2.4.4 Anti-Windup in the Integrator

In real life control systems a nonlinearity that can often occur, among many other ones, is the saturation, which can lead to an effect called integrator windup. This

phenomenon happens when the integral part of the PID tries to act on the steady-state error in this situation, causing to highly increase both the settling time and the overshoot in the step response, since the control error stays for a large amount of time at an opposite sign, in order to compensate the integrator and return it to the steady-state value (BOHN; ATHERTON, 1995). Different anti-windup techniques, such as back-calculation and clamping, were developed to deal with this effect and to guarantee that the controller will properly work.

2.4.4.1 Clamping

This anti-windup technique makes use of a switch connected to the integral part of the controller, in order to cancel the effect of the integration when the signal goes higher or lower than the previous set boundary values, consequently minimizing the windup phenomenon (JALIL et al., 2021). Figure 5 illustrates the schematic of the controller with clamping.

Figure 5 – Clamping Anti-Windup.

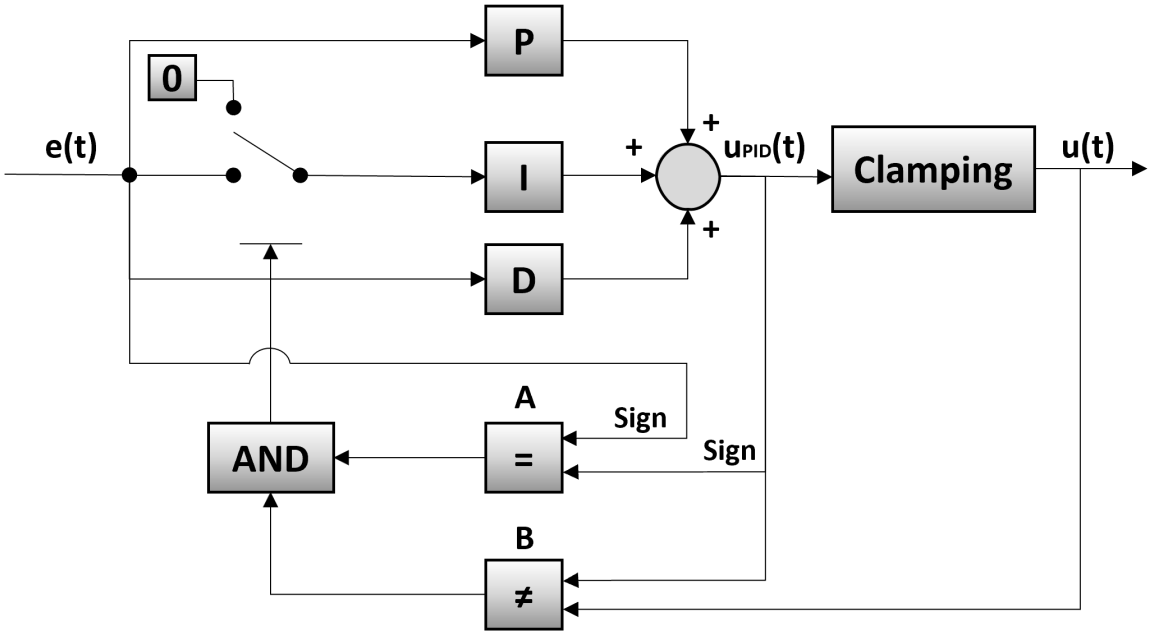

Source: Adapted from Astrom and Hagglund (2006)

Two operators are responsible for turning the switch on or off. Operator *A* compares the sign of the error $e(t)$ with the sign of the output from the PID $u_{PID}(t)$. If they have the same sign, it means that the error is increasing and it tends to increase more, or that the error is decreasing and it tends to decrease, depending on the signs being positive or negative. Operator *B* compares the actual value from the output of the controller $u_{PID}(t)$ with the output of the clamping block, which is the input value for the plant

$u(t)$. If they have the same value, it means that the saturation point was not reached yet. Otherwise, having different values means that the clamping is already acting on the saturation point. Table 2 illustrates the switch action based on the operators A and B.

Table 2 – Switch action in Clamping Anti-Windup.

Operator A	**Operator B**	**Switch**
sign $e(t)$ = sign $u_{PID}(t)$	$u_{PID}(t) \neq u(t)$	Off
sign $e(t)$ = sign $u_{PID}(t)$	$u_{PID}(t) = u(t)$	On
sign $e(t) \neq$ sign $u_{PID}(t)$	$u_{PID}(t) \neq u(t)$	On
sign $e(t) \neq$ sign $u_{PID}(t)$	$u_{PID}(t) = u(t)$	On

Source: Adapted from Jalil et al. (2021).

2.4.4.2 Back-calculation

The integral part of the controller is recalculated when the control signal reaches the saturation boundaries, to guarantee that its new value is within the limits. The system measures the error signal e_s by comparing the differences between the actuator output u and the controller output v, with the help of an additional feedback loop, as shown in Figure 6. In case the actuator does not saturate, no action is needed and the signal will be zero. On the contrary if it does reach the saturation point, the error signal is not zero and the closed-loop feedback is interrupted, since the input will remain the same (ÅSTRÖM; HÄGGLUND, 1995).

Figure 6 – Back-calculation Anti-Windup.

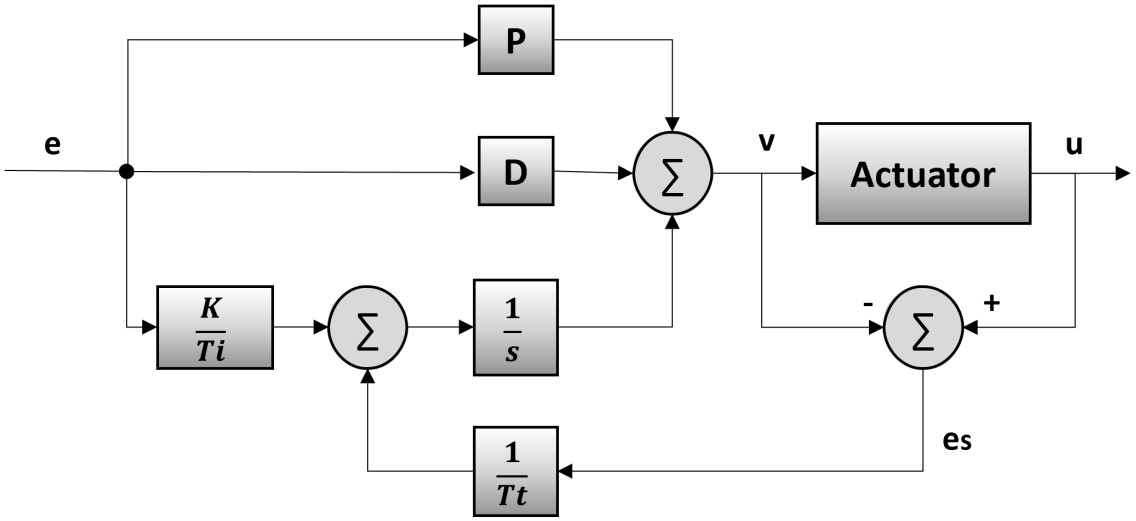

Source: Adapted from Åström and Hägglund (1995)

The inner feedback, from the back-calculation, is responsible for driving the integrator output to a certain value, which will cause the integrator input to become zero, as Equation (14) describes.

$$e\frac{K}{T_i} + e_s\frac{1}{T_t} = 0, \tag{14}$$

where T_t, called tracking time constant, is the time that determines when the integral will be reset, being $1/T_t$ the rate at which this happens, also known as the feedback gain for the back-calculation. By isolating e_s in Equation (14) and substituting it in $v = u - e_s$, the controller output can be described as Equation (15).

$$v = u_{lim} + e\frac{T_t K}{T_i}, \tag{15}$$

where u_{lim} is the saturating value of the control variable, which will always have a smaller magnitude than v, since e and u_{lim} have the same sign, protecting the integrator from the windup effect (ÅSTRÖM; HÄGGLUND, 1995).

2.5 STATE-SPACE REPRESENTATION

A Linear Time-Invariant (LTI) system can be represented as shown in equations Equation (16a) and Equation (16b)

$$\dot{\mathbf{x}}(t) = \mathbf{A}\mathbf{x}(t) + \mathbf{B}\mathbf{u}(t) \tag{16a}$$

$$\mathbf{y}(t) = \mathbf{C}\mathbf{x}(t) + \mathbf{D}\mathbf{u}(t), \tag{16b}$$

where $\mathbf{u}(t)$ and $\mathbf{y}(t)$ are respectively the input and output vectors, which contain variables used to actuate the system and measurable values, $\mathbf{x}(t)$ represents the state vector expressed by Equation (17) and contains internal system variables. The variables **A**, **B**, **C** and **D** are matrices that represent the system dynamics, input, output and direct transmission, in that order. The whole system representation is shown as a block diagram in Figure 7 (WILLIAMS; LAWRENCE, et al., 2007).

$$x(t) = \begin{bmatrix} x_1(t) \\ x_2(t) \\ \vdots \\ x_n(t) \end{bmatrix}. \tag{17}$$

Figure 7 – State-space representation in a block diagram.

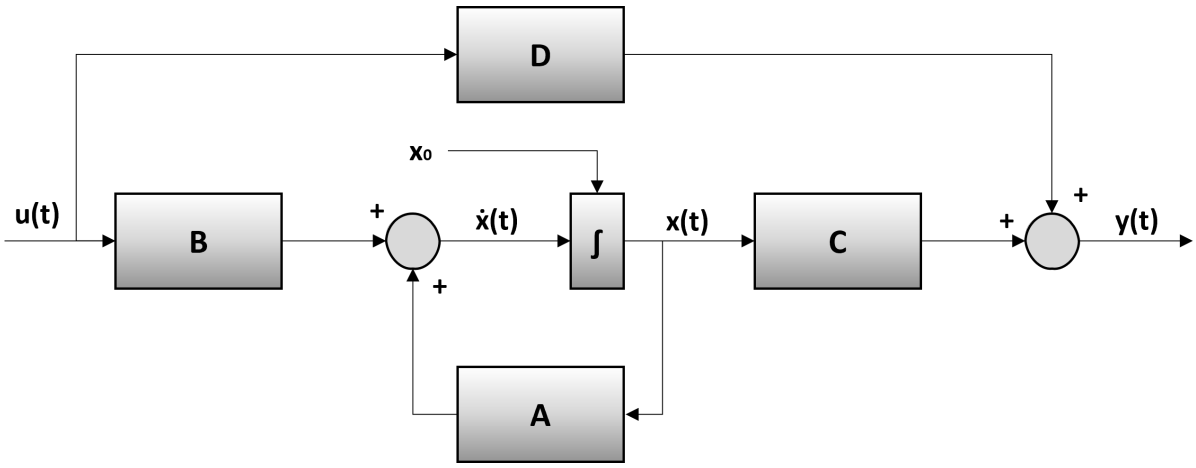

Source: Williams (2007, p. 5)

In the discrete-time with steps k the state-space model can be written as in Equation (18a) and Equation (18b)

$$\mathbf{x}_{k+1} = \mathbf{A}\mathbf{x}_k + \mathbf{B}\mathbf{u}_k \tag{18a}$$

$$\mathbf{y}_k = \mathbf{C}\mathbf{x}_k + \mathbf{D}\mathbf{u}_k. \tag{18b}$$

2.6 PID TUNING METHODS

In this section the two Ziegler-Nichols PID Tuning Methods will be discussed.

2.6.1 Ziegler-Nichols Methods

There are two methods that were developed by Ziegler and Nichols with the purpose of tuning a PID controller based on the step response and the oscillation state of the system, respectively.

2.6.1.1 First Ziegler-Nichols Method

In cases where the step response of the system is in the form illustrated by Figure 8, this method can be applied to tune the PID controller. Normally, this can be obtained from a first order system with a delay in time (MESHRAM; KANOJIYA, 2012). The transfer function for systems with this behaviour can be approximated by the Equation (19),

Figure 8 – Step response for Ziegler-Nichols Method.

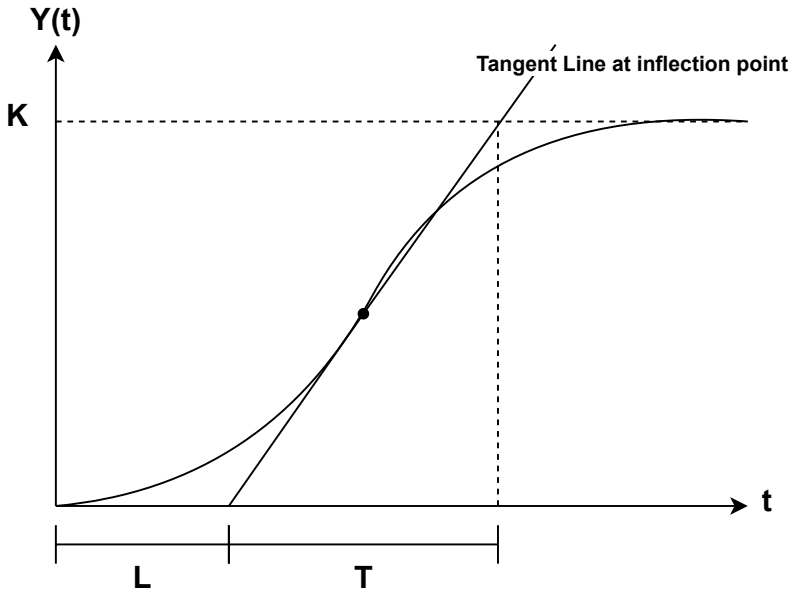

Source: Meshram (2012, p. 119)

$$G(s) = \frac{Ke^{-sL}}{Ts+1}, \tag{19}$$

where K is the gain in steady-state, L is the delay time and T is the time constant, as illustrated in Figure 8. With the values obtained from the step response, the Table 3 developed by Ziegler and Nichols is used to find the PID parameters, such as K_p, T_i and T_d, where $K_i = K_p/T_i$ and $K_d = K_p T_d$.

Table 3 – Ziegler-Nichols First Method tuning table.

Controller	K_p	T_i	T_d
P	$\frac{T}{KL}$	∞	0
PI	$0.9\frac{T}{KL}$	$\frac{L}{0.3}$	0
PID	$1.2\frac{T}{KL}$	$2L$	$0.5L$

Source: Brito (2019).

2.6.1.2 Second Ziegler-Nichols Method

The second Ziegler-Nichols method requires that an unstable state and sustained oscillations can be reached by changing the proportional portion of the controller. In case this state is not reachable or it can damage the system, this method cannot be

applied. The steps for this method consists in removing the integrator and derivative portions, which means setting them to zero, then increasing the proportional gain from zero until the system reaches the verge of instability, where sustained oscillations occur. The controller parameters are obtained from Table 4 developed by Ziegler and Nichols (COPELAND, 2008), where K_{cr} is the proportional gain where the sustained oscillations exist. The corresponding critical period for this point is the P_{cr} and it can be obtained in two different ways. The first one is by analyzing the step response of the system when $K_p = K_{cr}$ and measure the peak-to-peak distance, which means the period of the signal, as illustrated by Figure 9 (OGATA, 2001).

Table 4 – Ziegler-Nichols Second Method tuning table.

Controller	K_p	T_i	T_d
P	$0.5K_{cr}$		
PI	$0.45K_{cr}$	$\frac{P_{cr}}{1.2}$	
PID	$0.6K_{cr}$	$\frac{P_{cr}}{2}$	$\frac{P_{cr}}{8}$

Source: Copeland (2008).

Figure 9 – Step response for Second Ziegler-Nichols Method.

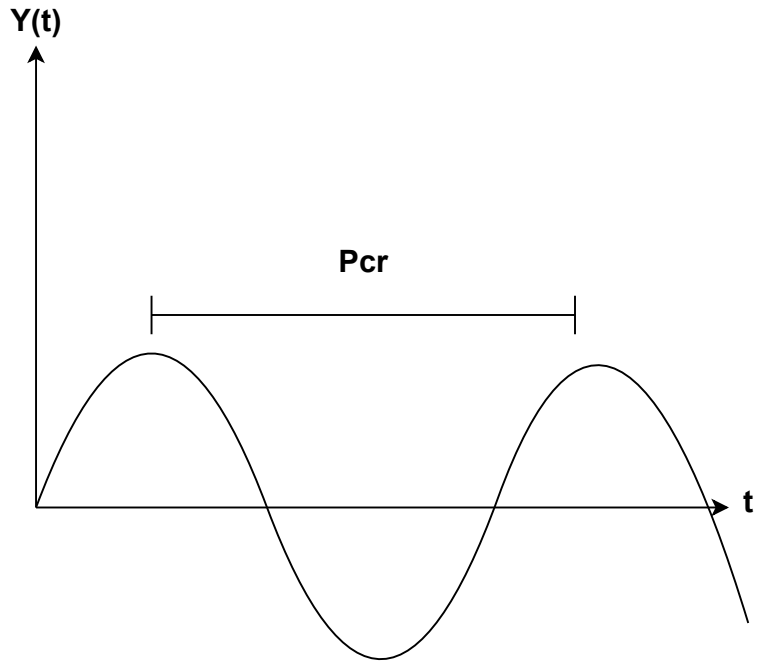

Source: Ogata (2001, p. 571)

The PID can now be written as Equation (20)

$$G_c(s) = 0.075 K_{cr} P_{cr} \frac{\left(s + \frac{4}{P_{cr}}\right)^2}{s}. \tag{20}$$

By analyzing Equation (20) it is possible to verify that the PID in this method has a pole at the origin and two zeros at $s = -4/P_{cr}$.

2.7 SINGULAR VALUE DECOMPOSITION

Commonly seen as a method for data reduction, the Singular Value Decomposition (SVD) consists in reducing a high dimensional set of data points to a lower dimensional space, ordered by the most variable to the least variable, demonstrating in a clearly way the substructure of that data. Based on a theorem from linear algebra and usually represented by Equation (21), the method can find where the most variation in a data set is located and based on that, find the most accurate approximation using less dimensions. The theorem states that a rectangular matrix A can be written as the product of an orthogonal matrix U, a diagonal matrix S and the transpose of an orthogonal matrix V (BAKER, 2005).

$$A_{mn} = U_{mm} S_{mn} V_{nn}^T. \tag{21}$$

The columns of U are orthonormal eigenvectors of AA^T, the columns of V are orthonormal eigenvectors of $A^T A$, and S is a diagonal matrix containing the square roots of the non-zero eigenvalues from U or V, spread in a descending order through the diagonal. The columns of U are called left singular vectors, the columns in V are the right singular vectors and those diagonal values are called the singular values from matrix A (BAKER, 2005).

2.8 SYSTEM IDENTIFICATION

In order to have a quality control design, a proper model that can accurately represent the dynamics of the system is necessary. This process of creating mathematical models based on input-output data, is known as system identification in the control area. Depending on the real life system, different techniques can be approached, such as linear, nonlinear and hybrid. It can be subdivided in three steps, obtain information data, estimation with a set of models and validation of the models (LJUNG, 2010).

The data from the real system required for the process is used in the beginning and at the end of the system identification. That happens because it is used at first

to build the models and at the end to validate the models created. After obtaining the data from the system, the model structure needs to be chosen. It is common to choose multiple structures and models to evaluate which reproduces the most accurate results. The model structures can be separated in three different types, the black-box structure, the structure from physical model and the structure from semi-physical model (LJUNG, 1998).

2.8.1 Eigensystem Realization Algorithm

Commonly used in high-dimensional systems and developed to identify structural models in the aerospace field, the Eigensystem Realization Algorithm (ERA) can be used to obtain a state-space model of a system from measurements of its impulse response, without having previous knowledge about the dynamics or physical aspects of it (BRUNTON; KUTZ, 2019). Considering the state-space description of a model in the discrete-time as shown in equations Equation (18a) and Equation (18b), and an impulse input in discrete-time represented by u_k^δ as in Equation (22),

$$\mathbf{u}_k^\delta = \begin{cases} \mathbf{I}, & k = 0 \\ \mathbf{0}, & k = 1, 2, 3, \cdots \end{cases}, \tag{22}$$

and the respective response in Equation (23)

$$\mathbf{y}_k^\delta = \begin{cases} \mathbf{D}, & k = 0 \\ \mathbf{CBA}^{k-1}, & k = 1, 2, 3, \cdots \end{cases}, \tag{23}$$

a Hankel matrix can be formed with the respective impulse response y_k^δ values measured from the sensors, as shown in Equation (24)

$$\mathbf{H} = \begin{bmatrix} \mathbf{y}_1^\delta & \mathbf{y}_2^\delta & \cdots & \mathbf{y}_{mc}^\delta \\ \mathbf{y}_2^\delta & \mathbf{y}_3^\delta & \cdots & \mathbf{y}_{mc+1}^\delta \\ \vdots & \vdots & \ddots & \vdots \\ \mathbf{y}_{mo}^\delta & \mathbf{y}_{mo+1}^\delta & \cdots & \mathbf{y}_{mc+mo-1}^\delta \end{bmatrix}. \tag{24}$$

By taking the SVD of the matrix, as illustrated in Equation (25), the matrix can be rewritten in terms of its dominant temporal patterns,

$$\mathbf{H} = \mathbf{U}\Sigma\mathbf{V}^* = \begin{bmatrix} \tilde{\mathbf{U}} & \mathbf{U}_t \end{bmatrix} \begin{bmatrix} \tilde{\Sigma} & \mathbf{0} \\ \mathbf{0} & \Sigma_t \end{bmatrix} \begin{bmatrix} \tilde{\mathbf{V}}^* \\ \mathbf{V}_t^* \end{bmatrix} \approx \tilde{\mathbf{U}}\tilde{\Sigma}\tilde{\mathbf{V}}^*, \tag{25}$$

where $\tilde{\mathbf{U}}$ and $\tilde{\mathbf{V}}$ are the eigen-time-delay coordinates and $\tilde{\Sigma}$ represents the singular values truncated in *r*, which means only the first *r* values are maintained. With that, it is possible to build the system matrices with reduced order, as Equation (26a), Equation (26b) and Equation (26c) show.

$$\tilde{\mathbf{A}} = \tilde{\Sigma}^{-1/2}\tilde{\mathbf{U}}^*\mathbf{H}^{'}\tilde{\mathbf{V}}\tilde{\Sigma}^{-1/2}; \tag{26a}$$

$$\tilde{\mathbf{B}} = \tilde{\Sigma}^{-1/2}\tilde{\mathbf{V}}^* \begin{bmatrix} \mathbf{I_p} & \mathbf{0} \\ \mathbf{0} & \mathbf{0} \end{bmatrix}; \tag{26b}$$

$$\tilde{\mathbf{C}} = \begin{bmatrix} \mathbf{I_q} & \mathbf{0} \\ \mathbf{0} & \mathbf{0} \end{bmatrix} \tilde{\mathbf{U}}\tilde{\Sigma}^{1/2}, \tag{26c}$$

where $\mathbf{I_p}$ and $\mathbf{I_q}$ are identity matrices, with the first *p* columns and the first *q* rows extracted, respectively. The matrix $\mathbf{H}^{'}$ is called the shifted Hankel matrix and is represented by Equation (27)

$$\mathbf{H}^{'} = \begin{bmatrix} \mathbf{y}_2^\delta & \mathbf{y}_3^\delta & \cdots & \mathbf{y}_{mc+1}^\delta \\ \mathbf{y}_3^\delta & \mathbf{y}_4^\delta & \cdots & \mathbf{y}_{mc+2}^\delta \\ \vdots & \vdots & \ddots & \vdots \\ \mathbf{y}_{mo+1}^\delta & \mathbf{y}_{mo+2}^\delta & \cdots & \mathbf{y}_{mc+mo}^\delta \end{bmatrix}. \tag{27}$$

The state-space model with reduced order can now be described by Equation (28a) and Equation (28b),

$$\tilde{\mathbf{x}}_{k+1} = \tilde{\mathbf{A}}\tilde{\mathbf{x}}_k + \tilde{\mathbf{B}}\mathbf{u} \tag{28a}$$

$$\mathbf{y} = \tilde{\mathbf{C}}\tilde{\mathbf{x}}_k. \tag{28b}$$

2.8.2 Observer Kalman Filter Identification

Since in some cases it is not an easy task to obtain the impulse response of a system, due to problems such as noise in the signal that can affect the result,

the Observer Kalman Filter Identification (OKID) method was created with the main characteristic of being an addition to the ERA, by approximating an impulse response from input-output data, which can then be used in the ERA method (BRUNTON; KUTZ, 2019).

The output y_k is now described by Equation (29).

$$y_k = C_d A_d^{k-1} B_d u_0 + C_d A_d^{k-2} B_d u_1 + \cdots + C_d B_d u_{k-1} + D_d u_k. \tag{29}$$

This output measurements from the system can be rewritten in a simplified form in terms of an impulse-response y_k^δ shown by Equation (30).

$$\begin{bmatrix} y_0 & y_1 & \cdots & y_m \end{bmatrix} = \begin{bmatrix} y_0^\delta & y_1^\delta & \cdots & y_m^\delta \end{bmatrix} \begin{bmatrix} u_0 & u_1 & \cdots & u_m \\ 0 & u_0 & \cdots & u_{m-1} \\ \vdots & \vdots & \ddots & \vdots \\ 0 & 0 & \cdots & u_0 \end{bmatrix}. \tag{30}$$

2.8.3 Nonlinear models

In this subsection some nonlinear models for Single Input Single Output (SISO) systems will be explained.

2.8.3.1 Hammerstein-Wiener model

The Hammerstein-Wiener is a model that consists of a dynamic linear block and two static nonlinear blocks in cascade, as illustrated in Figure 10

Figure 10 – Hammerstein-Wiener model.

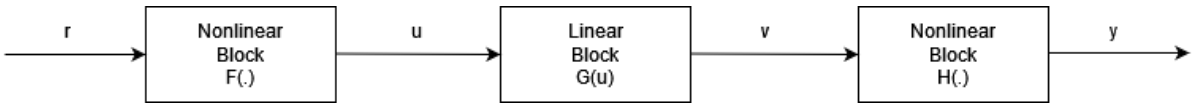

Source: Hong (2011, p. 236)

Mathematically, the model can be represented by the Equation (31)

$$y(k) = \sum_{i=1}^{n} a_i g(y(k-i)) + \sum_{j=1}^{m} b_j f(y(k-j)) + e(k). \tag{31}$$

2.8.3.2 Nonlinear ARX model

The Nonlinear ARX (NARX) can model dynamic nonlinearities, in opposition of the Hammerstein-Wiener model that can only model static nonlinearities. This model is an adaptation of the AutoRegressive with eXternal input (ARX) linear model, extending some important properties, such as the stability of its predictor in the identification of unstable systems and the characteristic of having efficient and trustworthy algorithms, since the solution of this model is calculated by the linear least-squares method (ZHU, 2002). Equation (32) represents the linear ARX model wrote in a linear regression form

$$y(t) = [1 - A(q)]y(t) + B(q)u(t) + e(t) = A^*(q)y(t) + B(q)u(t) + e(t), \tag{32}$$

where

$$\begin{cases} A(q) = 1 + a_1 q^{-1} + ... + a_n q^{-n} \\ A^*(q) = -a_1 q^{-1} + ... + -a_n q^{-n} \\ B(q) = b_1 q^{-1} + ... + b_n q^{-n}. \end{cases} \tag{33}$$

The input and output signals are respectively represented by $u(t)$ and $y(t)$. The model has a n_{th} order and a white noise $e(t)$ with zero mean. Besides that, the q^{-1} variable represents the unit delay operator. As stated by Zhu (2002), the reason why the model provides outstanding solutions is due to the error $e(t)$ being linear in the parameters, property that is also expanded to the nonlinear models, by adding an input and output nonlinear blocks, as shown in Equation (34)

$$y(t) = A^*(q)f_2[y(t)] + B(q)f_1[u(t)] + e(t). \tag{34}$$

The $f_1(t)$ and $f_2(t)$ terms represent respectively the input and output nonlinear blocks, which should be continuous functions. There are some special cases, such as when $f_2(t) = y$, in which case the nonlinear ARX turns into a Hammerstein model. By changing the order of the blocks and the polynomials, another three different and likely with more nonlinearities NARX models can be derived. (ZHU, 2002). A visual representation of this model, with the regressors and the linear and nonlinear output functions, can be seen in Figure 11.

Figure 11 – NARX model representation.

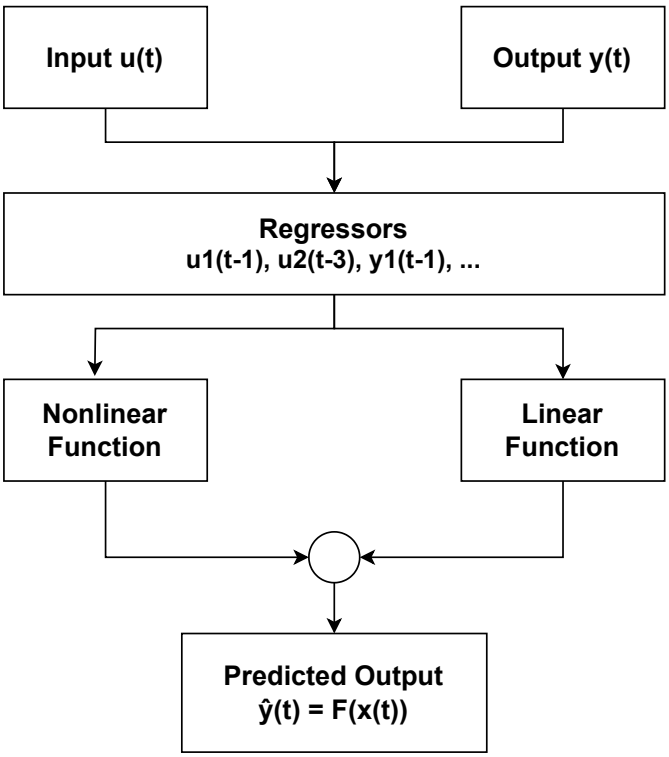

Source: Kumar (2010, p. 188)

The regressors, that can be represented by $x(t)$, are functions of the input-output data that was measured from the system, which means that the more knowledge about the system, the more precise the regressors can be, therefore the more accurate the model will be. The predicted output function $F(x(t))$ can be represented by Equation (35)

$$F(x) = \sum_{k=1}^{d} \alpha_k k(\beta_k(x - \gamma_k)), \tag{35}$$

where α_k, β_k and γ_k are the parameters of the nonlinearity estimators, k and d are respectively the unit nonlinear command and the number of nonlinearity units (KUMAR et al., 2010).

2.8.4 Problems with nonlinear models

Despite the currently advanced area that system identification has become, some problems still can be found. Even though the most active field is perhaps the identification of nonlinear models, many questions need to be raised, such as finding what are the useful parameterizations of the function, how to identify a nonlinear sys-

tem that operates in closed loop and is stabilized by an unknown regulator and how to find effective non-linearity tests based on the data. Another problem can be the model approximation or the model reduction, when trying to derive a model with sufficient accuracy from the data, being an approximation of the real description of the system (LJUNG, 2010).

The identification of linear systems is well understood, but when it comes to non-linear models, the challenge is usually bigger. To find descriptions that are adaptable enough to encompass a wide range of pertinent nonlinear phenomena while still allowing for the incorporation of physical knowledge in order to avoid being overly flexible is not a simple task. It is a complex process to provide a coherent analysis of the current system due to the several approaches and studies available in the area. Among those multiple approaches, a commonly used nomenclature exists to represent this spectrum of knowledge, such as white box, grey box and black box (LJUNG, 2010).

A white box approach is used when there is deep knowledge about the system and its dynamics and a physical model can be fully derived from first principles, such as physics, chemistry, biology or economy. The total opposite would be a black box approach, where no previous knowledge about the system is available or it is too complex to be understood, being based purely on the data measured from the real system. There is no direct connection between the model parameters and first principles, the modelling is done entirely with experimental data (NELLES, 2013).

In between those methods there is a variety of grey boxes, which is a combination of theoretical knowledge with quality data. The grey box approach can be subdivided in three different methods, called smoke-grey, steel-grey and slate-grey. The first one can be considered a semi-physical modeling, where the goal is to find a nonlinear transformation of the data that can better describe the system. A steel-grey box approach consists of a linearization around a point, by developing approximations in multiple areas close to each other, to deal with the nonlinearity. The last one is a combination between linear dynamic system and nonlinear static transformation and it can be a hybrid model or a block-oriented model, such as the Hammerstein-Wiener model (LJUNG, 2010).

3 METHODOLOGY

This section presents the environment in which the work was developed and the proposed system modeling.

3.1 ENVIRONMENT

The machine currently used for the PGM process in the Institute is from the Toshiba GMP series, represented by Figure 12, on the left the thermal model of the molding machine and on the right the mechanical model. It is composed by six parts in total, those parts being the upper and lower cooling plate, upper and lower mold, and upper and lower holder. Besides that, there are also six infrared lamps that are responsible for the heating of the system, three for upper parts and the other three for the lower parts. There is a sensor for measuring the temperature in one of the holders, which is the temperature that needs to be controlled in order to achieve the desired results from the glass molding.

The machine is connected to a PID controller, which is responsible for controlling the power of the infrared lamps necessary to achieve a certain heat rate, until it reaches the desired temperature values in the holder. There are multiple parameters to be set for the process, but the most important ones for this work are the temperature related ones, T_V and T_1, the soaking times ST_1 and ST_2, and also the temperature slopes G_V and G_1.

As illustrated by Figure 13 and explained in Chapter 2, the first step is the heating, which is subdivided in two parts. First, the temperature is raised from ambient to T_V with a rate of G_V Celsius degrees per second. After that, the temperature is raised with a rate of G_1 until it reaches T_1. The temperature is then maintained at T_1 for the total duration of ST_1 plus ST_2, before it starts the slow and fast cooling steps that will not be taken into consideration in the presented work.

The parameters and results of the experiments are saved in a web application, developed and hosted by the institute. The data read by the sensor is transferred from the machine to the software via the communication protocol Modbus and RS232, which is then sent to the Application Programming Interface (API) in the server via HyperText Transfer Protocol (HTTP) requests and stored in the database (ROCHA, 2020). Finally, the results of stored and live processes can be seen in the web application, as Figure 14 illustrates.

The Web App has stored all the experiments from the machine, with the corresponding set parameters and the results, such as the power and temperature values measured by the sensor. With that, it was possible to get multiple data to use in the modeling and also to compare the model results with the actual data. An example of experimental data obtained from the machine can be seen in Table 5.

Figure 12 – Toshiba GMP machine.

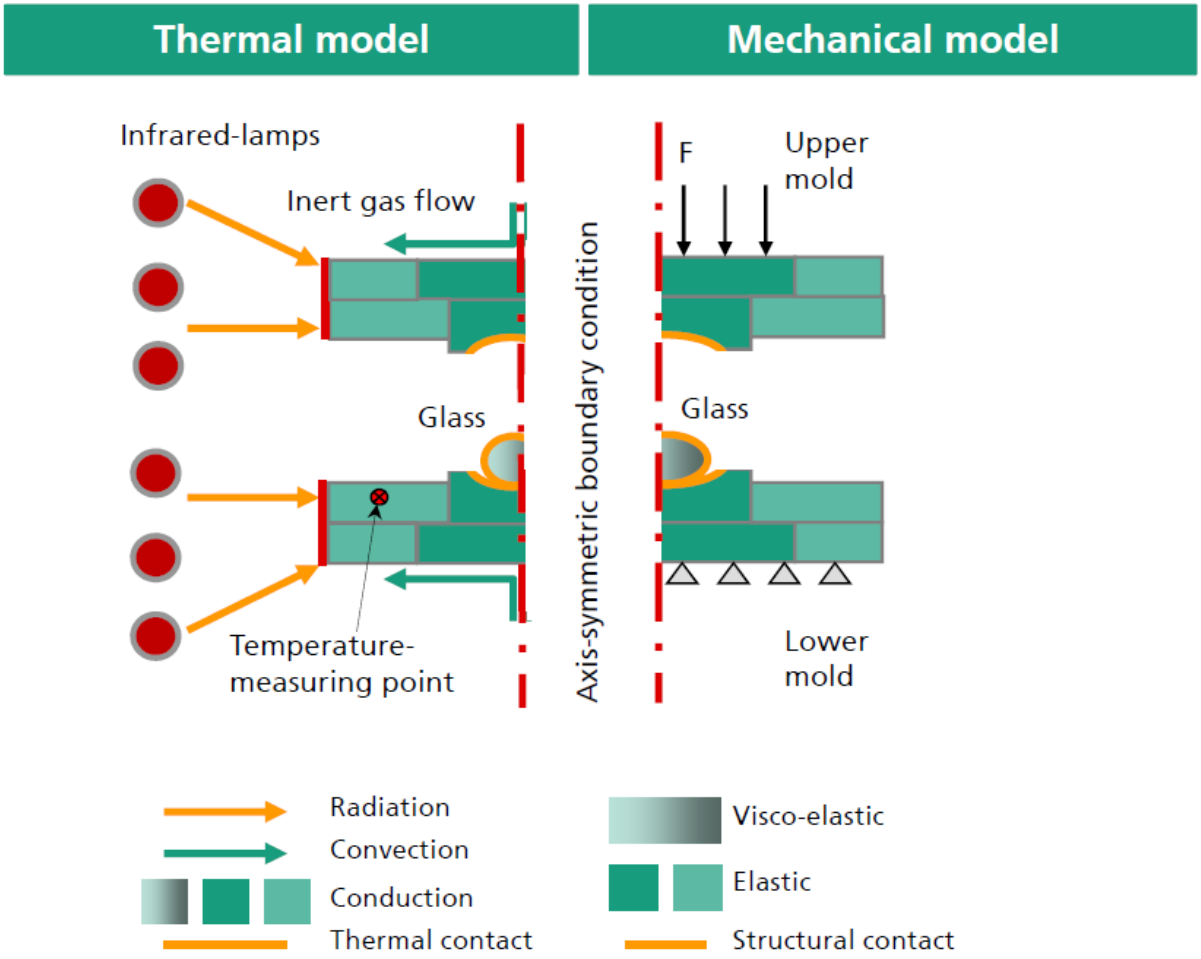

Source: Fraunhofer IPT's assets

Table 5 – Set parameters example table.

Process ID	**Temperature [℃]**		**Soaking Time [sec]**		**Temperature Slope [℃/sec]**	
	Tv	**T1**	**ST1**	**ST2**	**Gv**	**G1**
5932	480	560	300	200	3	0.5
5934	480	541	300	55	3	0.5
5935	480	539	300	124	3	0.5

Source: Author

Considering the machine tools and the infrared lamps to be a SISO system, where the input $u(t)$ is the infrared lamps power and the output $y(t)$ is the temperature rate in the holder, the first main goal was to find a model that could accurately represent this system, using the multiple experiments from the actual machine that were already available to be used for the process. The temperature rate (first G_V, then G_1) is the set value sent to the closed-loop system, in which the controller is responsible for changing

Figure 13 – PGM set parameters.

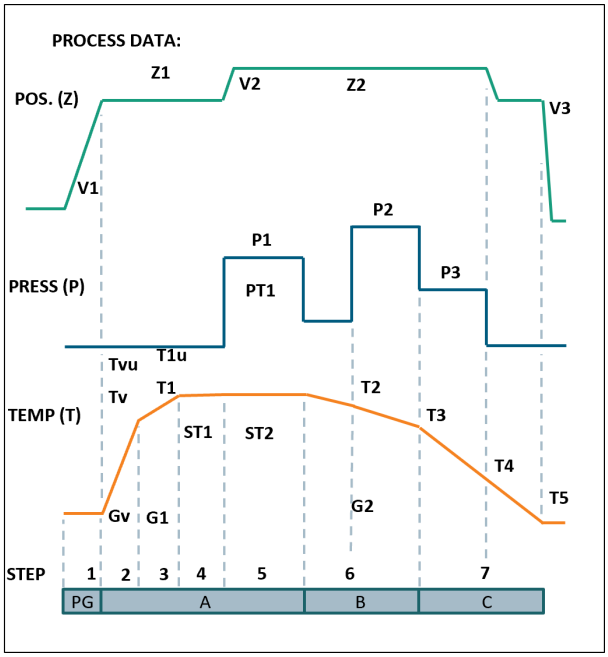

Source: Grunwald (2021, p. 53)

the lamp power and increase or decrease the temperature, in order to achieve the goal rate. This value is then read by the sensor and sent back in the feedback loop, as represented in Figure 15.

The input reference of the system $r(t)$ changes based on the temperature values T_V, T_1 and the current sensor temperature T_{sensor}. In other words, the controller tries to demand the necessary power in the lamps to keep the temperature rising at a certain rate, until it reaches the set values T_V and T_1, in this order. A simple logic was developed to calculate the temperature rate based on those values, to simulate the input of the closed-loop system, as illustrated by Equation (36),

$$r(t) = \begin{cases} G_V, & a > 0 \text{ and } b > 0 \\ G_1, & a \leq 0 \text{ and } b > 0 \\ 0, & a < 0 \text{ and } b \leq 0 \end{cases}, \tag{36}$$

where $a = T_V - T_{sensor}$ and $b = T_1 - T_{sensor}$. Figure 16 also demonstrates the result of the calculation. In the plot, the value t_{G_v} represents the point in time where the sensor temperature reaches the desired T_V value and consequently changes the rate. Similarly, the value t_{G_1} is the time where the sensor temperature reaches T_1 and after that, the soaking time period starts, where the temperature is held at a constant value, which

Figure 14 – Web App for visualization of PGM process.

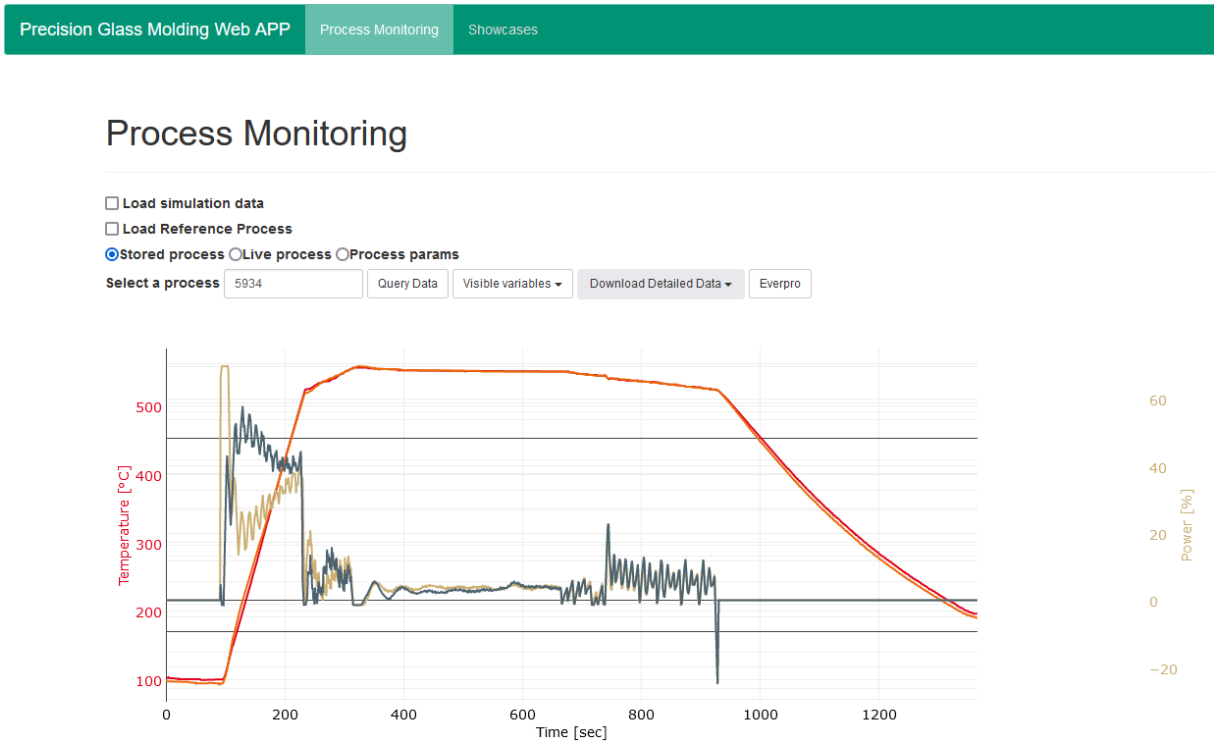

Source: Author

Figure 15 – Closed-loop representation of the system.

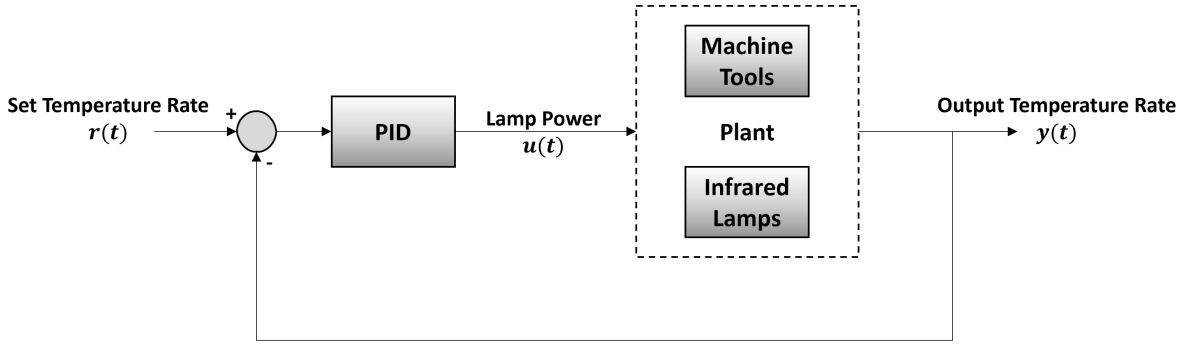

Source: Author

means the rate at this point is always zero, since there is no variation.

3.2 SYSTEM MODELING

One of the most common methods to model a real life system is deriving it from first principles by analyzing its dynamics. That means to use physical knowledge, such as Newton's laws, to mathematically describe the system (WANG, 2020). During the heating process, it is known that radiation is emitted by the infrared lamps and absorbed

Figure 16 – Input of the closed-loop system.

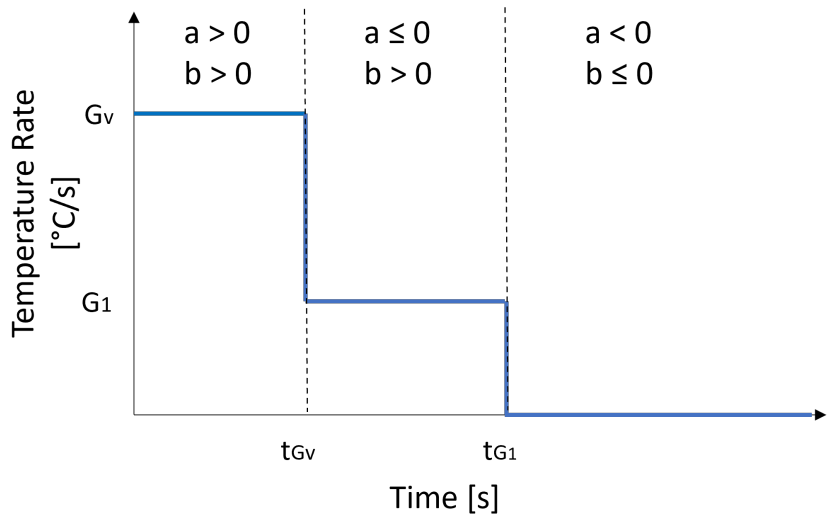

Source: Author

by the machine. Besides that, because of the contact between the machine parts and the nitrogen flow, heat is transferred by conduction and convection, respectively. The problem is that there is no other knowledge about the physics or the dynamics of the system and the information about it was not enough to derive a model using this method.

The First Ziegler-Nichols tuning method was then considered to be used for the identification of the system by using the approximation with a first order system with time delay. Since it was not possible to have access to the open-loop, which means have access to the system itself without the controller, the method could not be applied. Another comment on this procedure is that could be a problem to apply this technique, since the step response needs to be S-shaped, which may not occur in most cases.

The initial approach was to consider the system to be linear and consequently apply linear system identifications methods to verify if the results were close enough to the real data. This was done since the methods for linear systems are usually easier, which would avoid unnecessary work, and can possibly deliver good enough results. Alongside with the identification methods, the software Matlab was used for multiple steps, such as pre-processing, filtering, identifying, modeling and specially for simulating the generated models, with the help of Simulink. Figure 17 shows a Unified Modeling Language (UML) Activity diagram, to represent all the steps taken in the modeling process.

The first step was to pre-process the sensor data, since it has a lot of noise that can affect the identification of the system. Figure 18 illustrates one of the data used for the process as an example. The output temperature is in ℃ and the input power

Figure 17 – UML Activity diagram of the modeling process.

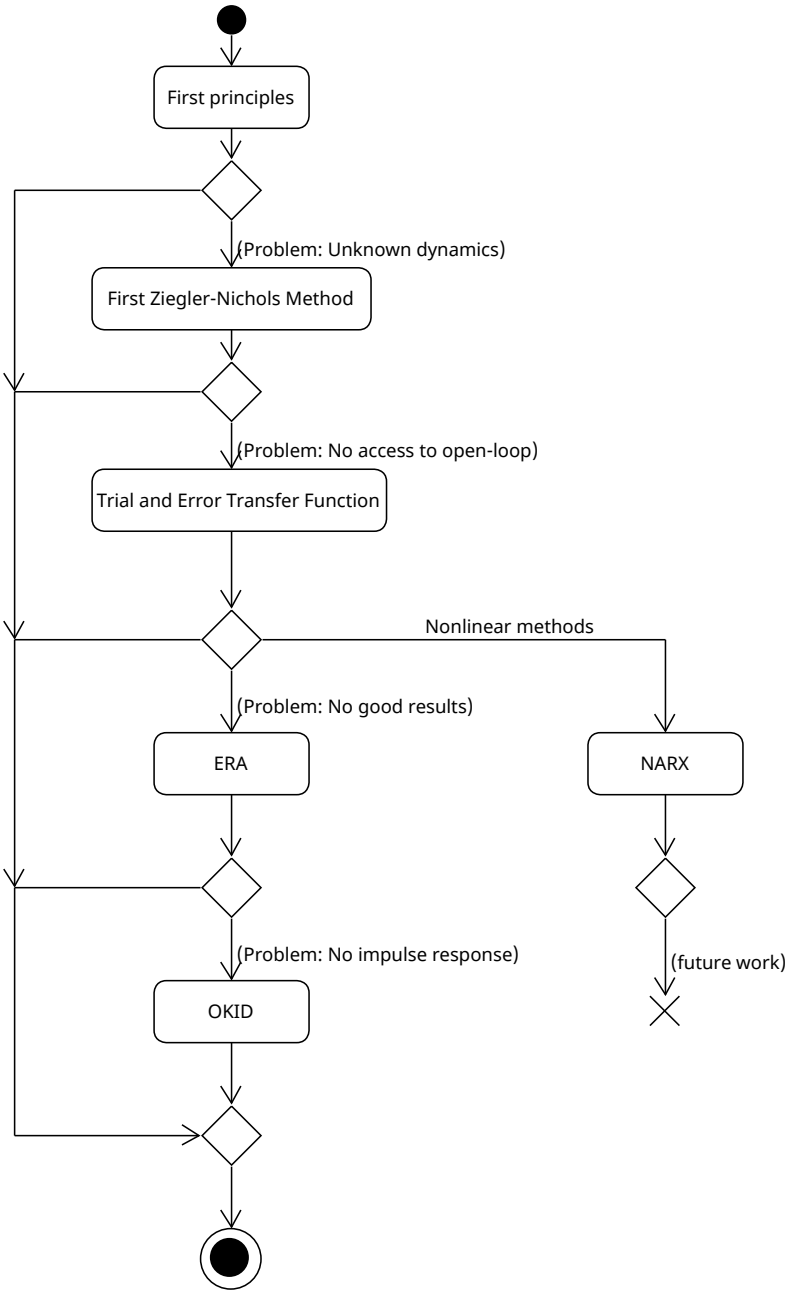

Source: Author

is in Watts. The whole process consists in multiple steps of heating and cooling, but since the presented work is focused on the heating, the cooling part was removed from the data. The temperature can usually start at room temperature or even a bit higher, when the machine has still not cooled down completely from previous experiments. This offset value was kept during the simulation, because if the temperature started at zero degrees, the model would have to compensate the difference by incrementing the power values and consequently the temperature rate, which would result in an

inaccurate modeling.

Figure 18 – Raw data from experiment.

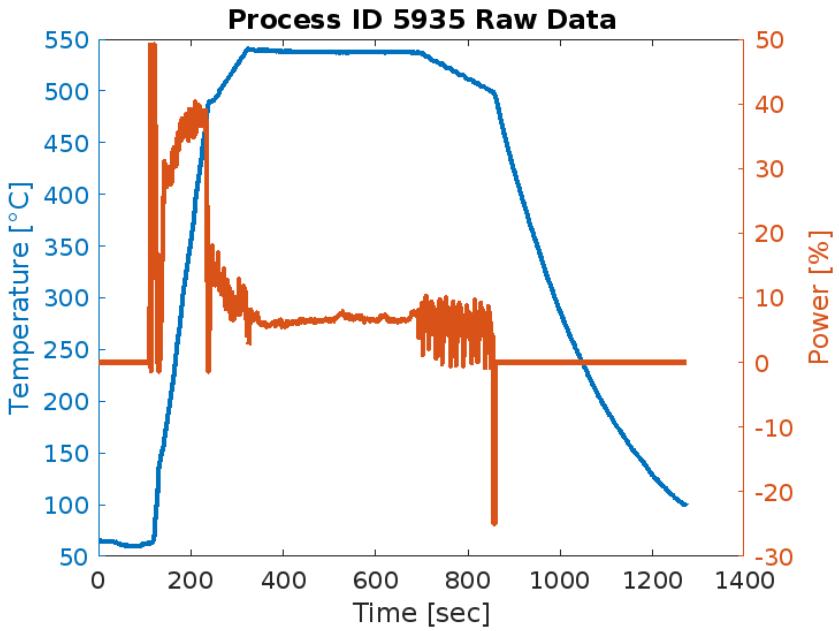

Source: Author

Even though the controller is responsible for the rate change, the values obtained from the experiments are actually measurements of the temperature in the holder, which means the derivative from these values were taken further in the simulation. The power data from the experiments is in percentage, from 0% until a maximum value, which was usually around 35 or 50%. There is three lamps in the upper position of the machine and three other in the lower position, and each lamp has a capacity of 3,3kW, which means the maximum power reachable is $3,3k * 3 = 9900W$ for each position.

The data from the experiments may contain some values below zero, which were removed, since it is evidently not physically possible to have negative percentage of power values, it represents noise or simply problems during the reading from the sensors. Figure 19 shows the post-processed signals used for the identification.

Since it was not possible to have access to the open-loop system, closed-loop identification techniques were addressed. The chosen method was the direct approach, where the assumption is to ignore the feedback and identify the open-loop with the input and output measurements (MANDLOI; SHAH, 2015). This option was chosen because it is possible to obtain measurements from inside the machine, the power values, and also the output temperature. The feedback is then not completely ignored, considering that it is not possible to remove the controller from the machine, which means the PID will be always acting on the plant.

Figure 19 – Post-processed input and output data from experiment.

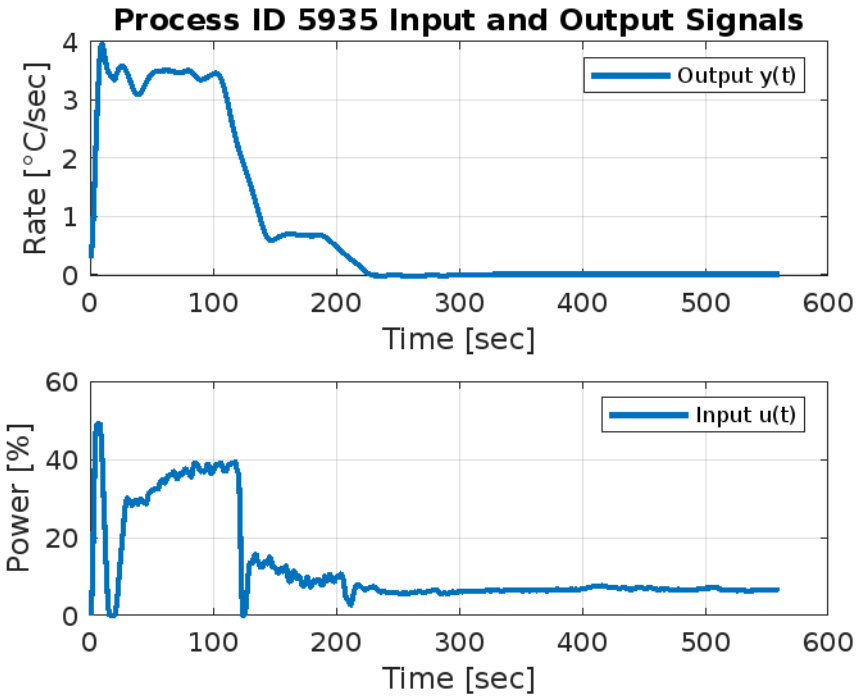

Source: Author

The first linear models were obtained by trial and error of different number of poles and zeros. The clear problem with this approach is that it is time consuming and there is no guarantee that a good model will be found. Different combinations of model orders were tested with Matlab, but the obtained models did not delivered satisfactory results.

The ERA method was then considered to obtain a state-space model of the system. This approach has two considerations, the first one being the assumption that the system is linear and can be described as Equation (16a) and Equation (16b) (or Equation (18a) and Equation (18b) for discrete-time). The other consideration is that an impulse response can be obtained, leading to the first problem during this procedure, since this requirement could not be met. A work-around for this was to first apply the OKID algorithm to extract an impulse response from random input-output data and then finally apply ERA.

The result from the OKID algorithm, which is the impulse response generated from the input-output data of the real system, is used to create the Hankel and shifted Hankel matrices in the ERA algorithm. After that, the SVD is taken and the Hankel singular values are obtained, which have a straight correlation with the model order. By plotting those singular values, the position to be truncated can be chosen based on where the values tend to acutely decrease. With Equation (26a), Equation (26b) and

Equation (26c), the system matrices represented in Equation (37) were obtained by using both the OKID and ERA algorithm provided by (BRUNTON; KUTZ, 2019).

$$\tilde{A} = \begin{bmatrix} -0.08 & -0.0812 & -0.031 & -0.009 \\ 0.0625 & 0 & 0 & 0 \\ 0 & 0.0625 & 0 & 0 \\ 0 & 0 & 0.0078 & 0 \end{bmatrix}, \tilde{B} = \begin{bmatrix} 0.125 \\ 0 \\ 0 \\ 0 \end{bmatrix}. \tag{37}$$
$$\tilde{C} = \begin{bmatrix} 0.077 & 0.048 & 0.026 & 0.0015 \end{bmatrix}, \tilde{D} = 0$$

In order to work with the rest of the system in closed-loop, the state-space model was converted into a transfer function, illustrated by Equation (38)

$$G(s) = \frac{0.009s^3 + 0.0004s^2 + 1.285e^{-5}s + 5.616e^{-9}}{s^4 + 0.08s^3 + 0.005s^2 + 0.0001s + 2.8e^{-7}}. \tag{38}$$

Since the power values have a specific range in the machine, it was necessary to limit the output of the PID with saturation values between zero and the upper limit percentage. To achieve this specific behavior in the model, an anti-windup technique could be used, to prevent the integrator part of the controller to output values outside the boundaries. The chosen method was the back-calculation with the tracking time constant T_t set to 1, which means the back-calculation coefficient K_b, that is the inverse of that time constant, was also 1.

The model obtained for the plant outputs the temperature rate, but since the temperature values from the sensor were available, a further step was needed to get the temperature from the predicted model, so that a proper comparison could be done. Besides that, there is an initial condition that needs to be considered, which is the fact that the temperature always starts at a certain value different than zero. Given the problems, the solution was to integrate the signal after the plant, with the initial condition of same temperature as the sensor data, to extract the temperature from the model. The Figure 20 illustrates in more details the final closed-loop system model.

Figure 20 – Full closed-loop system.

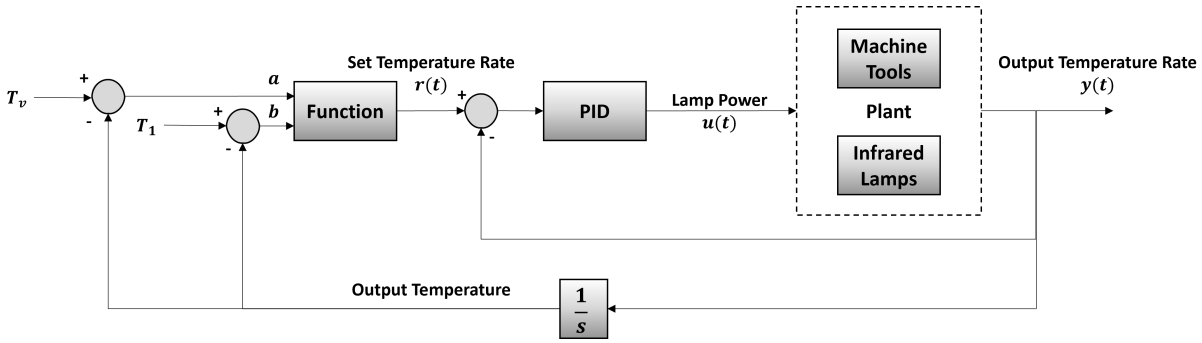

Source: Author

4 RESULTS

The process used to identify and model the system has the power and temperature measurements as already shown in chapter 3, before pre-processing in Figure 18 and after in Figure 19. The set parameters for this same process is also already shown in Table 5 in chapter 3. The linear model obtained from the ERA and OKID methods was used to run the simulations in Simulink.

After running the simulation in closed-loop with the PID using the same parameters from the machine, which means $K_P = 2.3$, $K_I = 55$ and $K_D = 3$, the results from the model for the reference (Figure 21), power (Figure 22a), temperature rate (Figure 22b) and temperature (Figure 22c) are obtained. The reference, as expected, starts at $G_V = 3$ ℃/s until it reaches $T_V = 480$ ℃, around 119 seconds. After that, it goes to $G_1 = 0.5$ ℃/s until 191 seconds, where the temperature reaches $T_1 = 539$ ℃. At last, the temperature rate drops down to zero and it is maintained, during the soaking time period, until the end of the simulation.

Figure 21 – Reference $r(t)$ for process 5935.

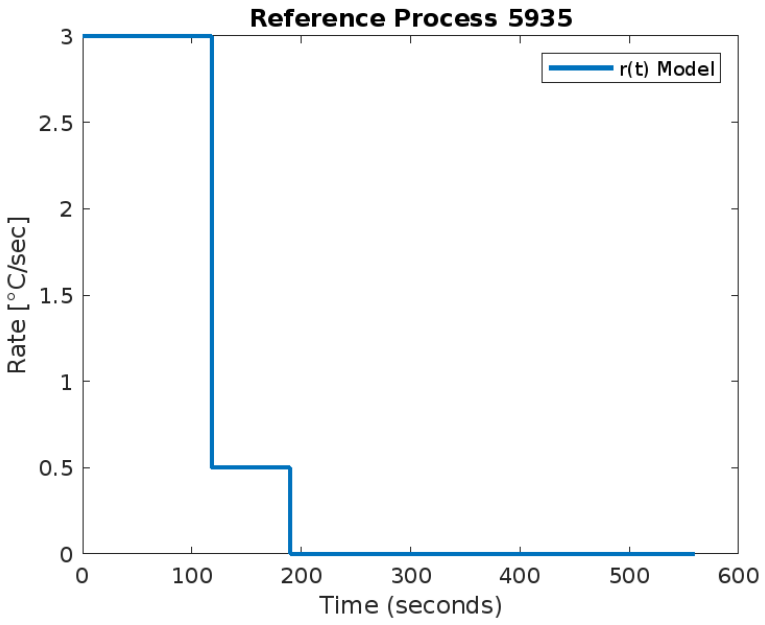

Source: Author

To calculate how good the predicted model response matches with the experimental data, the fit percentage was calculated with Equation (39), using the Normalized Root Mean Squared Error (NRMSE).

$$fit = 100(1 - NRMSE) = 100\left(1 - \frac{\|y - \hat{y}\|}{\|y - mean(y)\|}\right), \tag{39}$$

(a) Power values for process 5935.

(b) Temperature rate values for process 5935.

(c) Temperature values for process 5935.

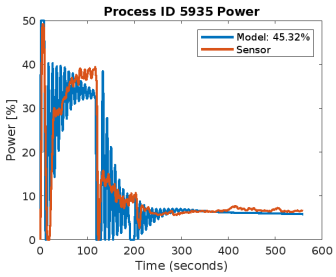

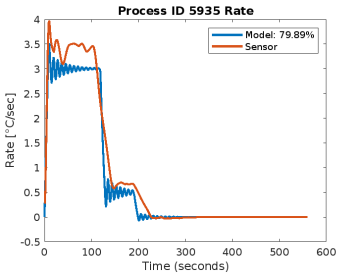

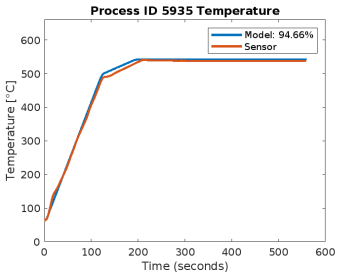

Source: Author

Source: Author

Source: Author

Figure 22 – Process 5935

where y is the experimental data and $\hat{y}$ is the output from the predicted model (THE MATHWORKS, 2023). Figure 22a illustrates the results for the power values, comparing the model output, in blue, with the actual sensor values, in orange. Even though the calculated fit shows that the model was not so accurate and the shape of the curve did not match in some parts, the margin of error set for the power values was achieved. Since the main goal was to model the system to control the temperature and temperature rate, at the moment the power fit was not as important as the other variables.

Figure 22b shows the results for the temperature rate values, once again the blue curve being the model output, and orange curve the sensor values. The calculated fit for the rate resulted in around 79.89%, which was satisfactory enough for the moment, compared to the sensor data and considering the maximum margin of error established.

Lastly, the calculated fit for the temperature from the predicted model was even better, resulting in around 94.66%, as Figure 22c illustrates. The end temperature from the model in the simulation was around 541.42 ℃, meaning a minor error of 0.63% compared to the experimental value.

Since the process 5935 was the one used for the modeling, it was necessary to compare the results with some validation data, using a different process. The process with ID 5934 was used to validate the predicted model. Its set parameters can also be seen in Table 5 in chapter 3 and the PID parameters were the same as process 5935. Figure 23a, Figure 23b and Figure 23c show the results for power, rate and temperature, respectively.

Process ID 5932 was also used as validation data to calculate the fit of the model. As the other processes, its set parameters are shown in Table 5 in chapter 3, and the PID parameters also the same as the others. Figure 24a, Figure 24b and Figure 24c illustrate the results. An interesting point to notice here is that the temperature fit for

(a) Power values for process 5934.

(b) Temperature rate values for process 5934.

(c) Temperature values for process 5934.

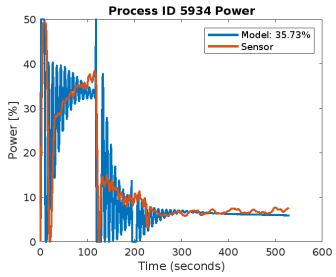

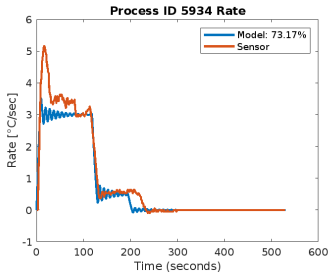

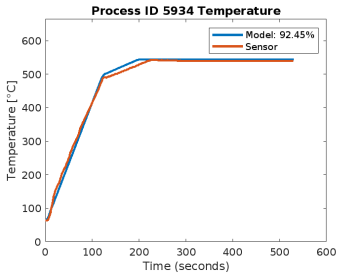

Source: Author

Source: Author

Source: Author

Figure 23 – Process 5934

(a) Power values for process 5932.

(b) Temperature rate values for process 5932.

(c) Temperature values for process 5932.

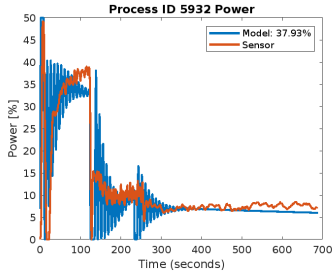

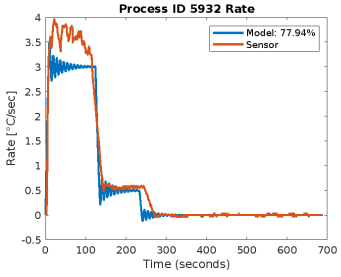

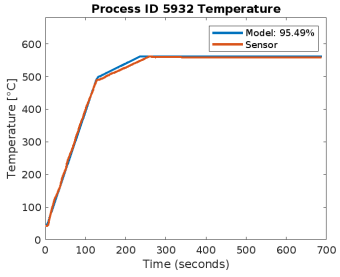

Source: Author

Source: Author

Source: Author

Figure 24 – Process 5932

this process was the best one, even better than the process that was used to generate the model.

The model obtained and both the training and validation data used was from the upper part of the machine. Even though the values from the upper and lower are very similar, it was necessary to validate if the predicted model performs well also with lower data, since there are three infrared lamps in the lower part as well. Figure 25 illustrates the results of validation using the lower data of the process used to obtain the model.

The reason for the outstanding difference in the power overall in all processes can be that it is possible to have different values in order to achieve the same temperature. As long as the desired rate and temperature are reached and the shape of the curve is maintained, the power can have different values. This is possible to observe by analysing the sensor data, where the temperature curve from different processes are almost the same, but the power can differ. Figure 26 illustrates an overview of the calculated fit percentages for each process and variables.

(a) Power values for process 5935 lower.

(b) Temperature rate values for process 5935 lower.

(c) Temperature values for process 5935 lower.

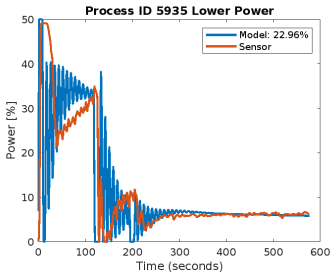

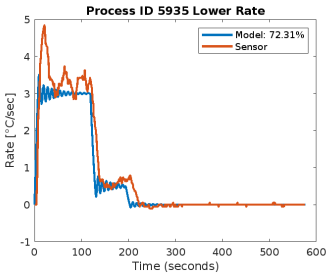

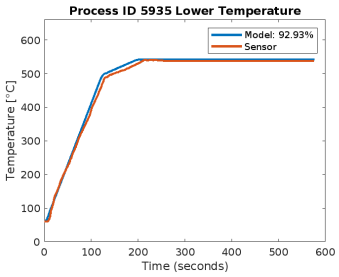

Source: Author

Source: Author

Source: Author

Figure 25 – Process 5935 Lower

Figure 26 – Overview of calculated fit for each process.

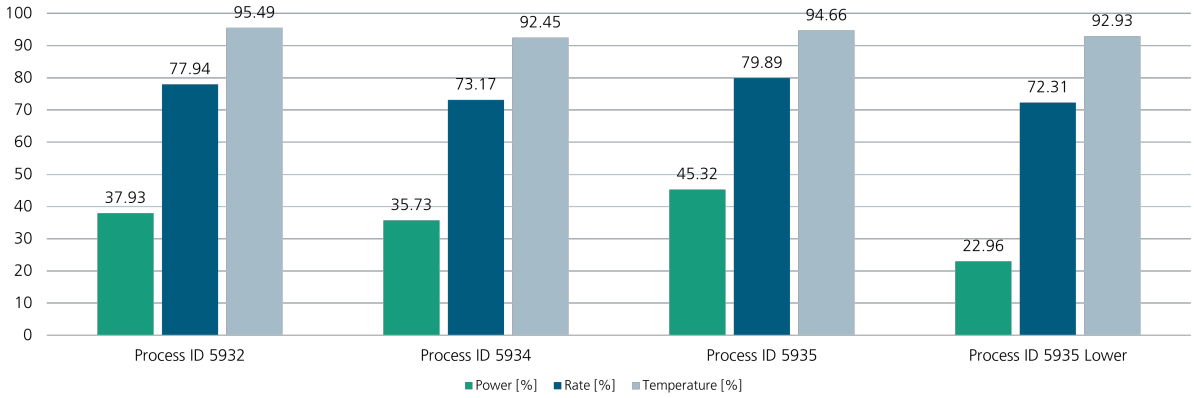

Source: Author

Lastly, a simulation in the FEM software used in the institute was performed with the same parameters as the model, with the goal of showing an application example, which means how to use the predicted model and what are the advantages of it. One of the advantages is that the infrared lamps in the FEM simulation is not necessary anymore. Instead it is possible use the input process parameters in the model and use its output results as a boundary condition in the surface of the machine in the simulation. Besides that, another advantage is that the tuning of the controller can now be done in the Simulink model, avoiding the time consume of doing it in the real machine. Figure 27 illustrates a comparison between the model and the FEM simulation results, before and after, using the model results.

Figure 27 – FEM simulation and model results.

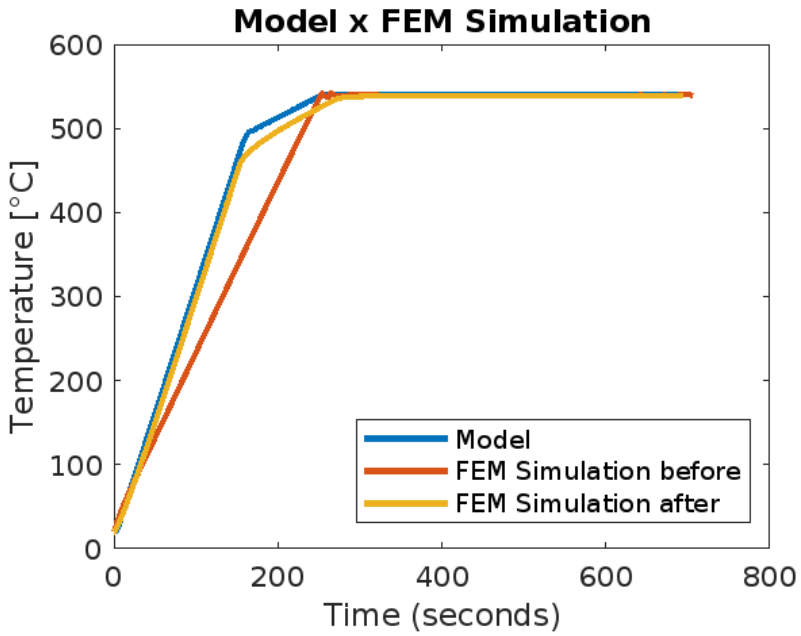

Source: Author

5 CONCLUSIONS

The proposed work had the goal to identify a correlation between the lamp power and the tools temperature, by modeling the machine responsible for the PGM process and its components as a control system. The reason for that is to better understand the PID controller, since it is time consuming to tune it, and to easily simulate the heating process with more precision. At first, the linear methods developed did not delivered satisfactory results, which lead to a different approach. The study of nonlinear systems and nonlinear system identification techniques were extensively addressed, such as the Hammerstein-Wiener and the NARX models. The results were promising but some problems were encountered, which was how to linearize this systems to later work together with the controller and how to obtain the best model without overfitting the training data. Because of the time constraint, those problems could not be solved and are left for future work. One more relevant topic is that in this work the system was modeled as a SISO system, but since the infrared lamps are positioned both in the upper and lower parts of the machine, one can have affect on the other, so a Multiple Input Multiple Output (MIMO) system could also be considered in future works. After trying many different techniques, the predicted model was shown to have good results and a good overall fit to the experimental data from multiple processes, proving that an digital twin for the PGM process can be developed and that the temperature in the infrared lamps during the heating step can be controlled based on input process parameters.

REFERENCES

24CHEMICALRESEARCH. **Precision Glass Molding Market Insights, Forecast to 2025**. North Main Road Koregaon Park, Pune, India - 411001: 24chemicalresearch, 2019. Available from: https://www.24chemicalresearch.com/reports/33837/precision-glass-molding-2025-611.

ASTROM, Karl J; HAGGLUND, Tore. **Advanced PID control**. Advanced PID control: ISA, 2006. Available from: https://cds.cern.ch/record/1514097.

ÅSTRÖM, Karl Johan; HÄGGLUND, Tore. **PID Controllers: Theory, Design, and Tuning**. [S.l.]: ISA - The Instrumentation, Systems and Automation Society, 1995. ISBN 1-55617-516-7.

BAKER, Kirk. Singular value decomposition tutorial. **The Ohio State University**, v. 24, 2005.

BÖCKH, Peter von; WETZEL, Thomas. Thermal radiation. In: HEAT Transfer: Basics and Practice. Berlin, Heidelberg: Springer Berlin Heidelberg, 2012. P. 189–213. ISBN 978-3-642-19183-1. DOI: 10.1007/978-3-642-19183-1_7. Available from: https://doi.org/10.1007/978-3-642-19183-1_7.

BOHN, C.; ATHERTON, D.P. An analysis package comparing PID anti-windup strategies. **IEEE Control Systems Magazine**, v. 15, n. 2, p. 34–40, 1995. DOI: 10.1109/37.375281.

BRITO, Alexandro Garro. On the misunderstanding of the Ziegler-Nichols formulae usage. **IEEE/CAA Journal of Automatica Sinica**, v. 6, n. 1, p. 142–147, 2019. DOI: 10.1109/JAS.2019.1911336.

BRUNTON, Steven L.; KUTZ, J. Nathan. **Data-Driven Science and Engineering: Machine Learning, Dynamical Systems, and Control**. [S.l.]: Cambridge University Press, 2019. DOI: 10.1017/9781108380690.

BURMEISTER, L.C. **Convective Heat Transfer**. [S.l.]: Wiley, 1993. (Wiley-Interscience publication). ISBN 9780471577096. Available from: https://books.google.de/books?id=pJaiReRZvHMC.

COPELAND, Brian R. The design of PID controllers using Ziegler Nichols tuning. **Zieglar-Nicholos Method**, 2008.

DAMBON, Olaf; WANG, Fei; KLOCKE, Fritz; PONGS, Guido; BRESSELER, Bernd; CHEN, Yang; YI, Allen Y. Efficient mold manufacturing for precision glass molding. **Journal of Vacuum Science & Technology B: Microelectronics and Nanometer Structures Processing, Measurement, and Phenomena**, v. 27, n. 3, p. 1445–1449, 2009. DOI: 10.1116/1.3056171. Available from: https://avs.scitation.org/doi/abs/10.1116/1.3056171.

DHATT, Gouri; LEFRANÇOIS, Emmanuel; TOUZOT, Gilbert. **Finite element method**. [S.l.]: John Wiley & Sons, 2012.

DONG, Xiaohu; LIU, Huiqing; CHEN, Zhangxin. Chapter 3 - Calculations of wellbore heat loss. In: DONG, Xiaohu; LIU, Huiqing; CHEN, Zhangxin (Eds.). **Hybrid Enhanced Oil Recovery Processes for Heavy Oil Reservoirs**. [S.l.]: Elsevier, 2021. v. 73. (Developments in Petroleum Science). P. 99–135. Available from: https://www.sciencedirect.com/science/article/pii/B9780128239544000060.

FENNER, R.T. **Finite Element Methods For Engineers (2nd Edition)**. [S.l.]: World Scientific Publishing Company, 2013. ISBN 9781908979674. Available from: https://books.google.de/books?id=d-s7DQAAQBAJ.

GRUNWALD, Tim. **Modellierung des Werkzeugverschleißes bei der Quarzglasumformung**. [S.l.]: Apprimus Wissenschaftsverlag, 2021.

HONG, Man; CHENG, Shao. Hammerstein-Wiener Model Predictive Control of Continuous Stirred Tank Reactor. In: HU, Wensong (Ed.). **Electronics and Signal Processing**. Berlin, Heidelberg: Springer Berlin Heidelberg, 2011. P. 235–242.

IPT, Fraunhofer. **Fine Machining and Optics**. 2022a. Available from: https://www.ipt.fraunhofer.de/en/Competencies/processtechnology/Finemachiningandoptics.html. Visited on: 16 Nov. 2022.

IPT, Fraunhofer. **The Fraunhofer IPT - a profile**. 2022b. Available from: https://www.ipt.fraunhofer.de/en/Profile.html. Visited on: 15 Nov. 2022.

IQBAL, Waqas. Identifying the optimum process parameters of precision glass molding for aspherical lenses, 2009. Available from: https://tigerprints.clemson.edu/all_theses/687/.

JALIL, Mohd Hafiz A.; HAMDAN, Rohaiza; NGADENGON, Rafidah; SHARIFF, Haslizamri Md; AMELY JUMAAT, Siti; ISLAM, Syed Zahurul. PID with Clamping Anti-windup Performance on Temperature Regulation of Glycerin Bleaching Process. In: 2021 IEEE 12th Control and System Graduate Research Colloquium (ICSGRC). [S.l.: s.n.], 2021. P. 127–131. DOI: 10.1109/ICSGRC53186.2021.9515200.

JOHNSON, M.A. PID Control Technology. In: **PID Control: New Identification and Design Methods**. Ed. by Michael A. Johnson and Mohammad H. Moradi. London: Springer London, 2005. P. 1–46. ISBN 978-1-84628-148-8. DOI: 10.1007/1-84628-148-2_1. Available from: https://doi.org/10.1007/1-84628-148-2_1.

KUMAR, Parmod; POTLURI, Chandrasekhar; SAB, An; CHIU, Steve; URFER, Alex; NAIDU, Desineni; SCHOEN, Marco. An adaptive multi sensor data fusion with hybrid nonlinear ARX and Wiener-Hammerstein models for skeletal muscle force estimation. In: p. 186–191.

LEVENSPIEL, Octave. The Three Mechanisms of Heat Transfer: Conduction, Convection, and Radiation. In: ENGINEERING Flow and Heat Exchange. Boston, MA: Springer US, 2014. P. 179–210. DOI: 10.1007/978-1-4899-7454-9_9. Available from: https://doi.org/10.1007/978-1-4899-7454-9_9.

LJUNG, Lennart. Perspectives on system identification. **Annual Reviews in Control**, v. 34, n. 1, p. 1–12, 2010. ISSN 1367-5788. DOI: https://doi.org/10.1016/j.arcontrol.2009.12.001. Available from: https://www.sciencedirect.com/science/article/pii/S1367578810000027.

LJUNG, Lennart. System Identification. In: **Signal Analysis and Prediction**. Ed. by Ales Procházka, Jan Uhlíř, P. W. J. Rayner and N. G. Kingsbury. Boston, MA: Birkhäuser Boston, 1998. P. 163–173. ISBN 978-1-4612-1768-8. DOI: 10.1007/978-1-4612-1768-8_11. Available from: https://doi.org/10.1007/978-1-4612-1768-8_11.

MANDLOI, Rohan; SHAH, Pritesh. Methods for closed loop system identification in industry. **Journal of Chemical and Pharmaceutical Research**, v. 7, n. 1, p. 892–896, 2015.

MESHRAM, P. M.; KANOJIYA, Rohit G. Tuning of PID controller using Ziegler-Nichols method for speed control of DC motor. In: IEEE-INTERNATIONAL Conference On Advances In Engineering, Science And Management (ICAESM -2012). [S.l.: s.n.], 2012. P. 117–122.

MUSA, Sumaila. Implementation of a PID-Controller on a Hardware Quadcopter System using dSPACE Platform. v. 5, May 2018. DOI: 10.21535/just.v5i3.993.

NELLES, Oliver. **Nonlinear System Identification**. Heidelberg: Springer Berlin, 2013.

OGATA, Katsuhiko. **Modern Control Engineering**. 4th. USA: Prentice Hall PTR, 2001. ISBN 0130609072.

ROCHA, Leonardo Pavan. **Simulation-based optimization of a precision glass molding thermal process**. 2020. BA thesis – Federal University of Santa Catarina.

THE MATHWORKS, Inc. **Compare identified model output with measured output**. 2023. Available from: https://de.mathworks.com/help/ident/ref/compare.html. Visited on: 12 June 2023.

WANG, Liuping. PID Control of Nonlinear Systems. In: PID Control System Design and Automatic Tuning using MATLAB/Simulink. [S.l.: s.n.], 2020. P. 179–202. DOI: 10.1002/9781119469414.ch6.

WHITELEY, Jonathan. An Overview of the Finite Element Method. In: FINITE Element Methods: A Practical Guide. Cham: Springer International Publishing, 2017. P. 1–4. ISBN 978-3-319-49971-0. DOI: 10.1007/978-3-319-49971-0_1. Available from: https://doi.org/10.1007/978-3-319-49971-0_1.

WILLIAMS, Robert L; LAWRENCE, Douglas A, et al. **Linear state-space control systems**. [S.l.]: John Wiley & Sons, 2007.

YAN, Jiwang; ZHOU, Tianfeng; MASUDA, Jun; KURIYAGAWA, Tsunemoto. Modeling high-temperature glass molding process by coupling heat transfer and viscous deformation analysis. **Precision Engineering**, v. 33, n. 2, p. 150–159, 2009. ISSN

0141-6359. DOI: https://doi.org/10.1016/j.precisioneng.2008.05.005. Available from: https://www.sciencedirect.com/science/article/pii/S0141635908000858.

ZHANG, L.; LIU, W. Precision glass molding: Toward an optimal fabrication of optical lenses. **Front. Mech. Eng.**, v. 12, 3–17, 2017. Available from: https://link.springer.com/article/10.1007/s11465-017-0408-3.

ZHANG, Yingying; LIANG, Rongguang; MILSTER, Tom D. A simulation-based optimization approach for the heating process of precision glass molding. In: OSA Optical Design and Fabrication 2021 (Flat Optics, Freeform, IODC, OFT). [S.l.]: Optica Publishing Group, 2021. otu5b.2. DOI: 10.1364/OFT.2021.OTu5B.2. Available from: https://opg.optica.org/abstract.cfm?URI=OFT-2021-OTu5B.2.

ZHU, Yucai. Estimation of nonlinear ARX models. In: PROCEEDINGS of the 41st IEEE Conference on Decision and Control, 2002. [S.l.: s.n.], 2002. 2214–2219 vol.2. DOI: 10.1109/CDC.2002.1184860.